Swiss J Geosci (2010) 103:293–315
DOI 10.1007/s00015-010-0019-z

Bentho-planktonic evidence from the Austrian Alps for a decline in sea-surface carbonate production at the end of the Triassic

Marie-Emilie Clémence · Silvia Gardin · Annachiara Bartolini · Guillaume Paris · Valérie Beaumont · Jean Guex

Received: 30 November 2009 / Accepted: 20 February 2010 / Published online: 24 August 2010

Abstract A high-resolution micropalaeontological study, combined with geochemical and sedimentological analyses was performed on the Tiefengraben, Schlossgraben and Eiberg sections (Austrian Alps) in order to characterize sea-surface carbonate production during the end-Triassic crisis. At the end-Rhaetian, the dominant calcareous nannofossil *Prinsiosphaera triassica* shows a decrease in abundance and size and this is correlated with a increase in $\delta^{18}O$ and a gradual decline in $\delta^{13}C_{carb}$ values. Simultaneously, benthic foraminiferal assemblages show a decrease in diversity and abundance of calcareous taxa and a dominance of infaunal agglutinated taxa. The smaller size of calcareous nannofossils disturbed the vertical export balance of the biological carbon pump towards the sea-bottom, resulting in changes in feeding strategies within the benthic foraminiferal assemblages from deposit feeders to detritus feeders and bacterial scavengers. These micropalaeontological data combined with geochemical proxies suggest that changes in seawater chemistry and/or cooling episodes might have occurred in the latest Triassic, leading to a marked decrease of carbonate production. This in turn culminated in the quasi-absence of calcareous nannofossils and benthic foraminifers in the latest Triassic. The aftermath (latest Triassic earliest Jurassic) was characterised by abundance peaks of "disaster" epifaunal agglutinated foraminifera *Trochammina* on the sea-floor. Central Atlantic Magmatic Province (CAMP) paroxysmal activity, superimposed on a major worldwide regressive phase, is assumed to be responsible for a deterioration in marine palaeoenvironments. CAMP sulfuric emissions might have been the trigger for cooling episodes and seawater acidification leading to disturbance of the surface carbonate production at the very end-Triassic.

Keywords Benthic foraminifera · Calcareous nannofossils · Carbonate production · End-Triassic crisis · CAMP volcanism · Austrian Alps

Editorial handling: Daniel Marty.

M.-E. Clémence · S. Gardin (✉)
Université de Paris VI, CR2P "Centre de Recherche sur la Paléobiodiversité et les Paléoenvironnements" CNRS UMR 7207, 4 place Jussieu, 75252 Paris Cedex 05, France
e-mail: silvia.gardin@upmc.fr

A. Bartolini
Muséum National d'Histoire Naturelle, CR2P "Centre de Recherche sur la Paléobiodiversité et les Paléoenvironnements" CNRS UMR 7207, 8 rue Buffon, 75231 Paris Cedex 05, France

G. Paris · V. Beaumont
Département de Géologie et Géochimie, IFP, 92852 Rueil Malmaison Cedex, France

J. Guex
IGP, Quartier UNIL-Dorigny, Bâtiment Anthropole 3182, 1015 Lausanne, Switzerland

Introduction

The Triassic-Jurassic (Tr-J) transition was a prolonged episode of biotic decline associated with important global environmental changes (Tanner et al. 2004), such as widespread igneous activity in the Central Atlantic Magmatic Province (CAMP; Marzoli et al. 1999), rapid sea-level fluctuations (Hallam and Wignall 1997; Hallam 2002), and large-scale perturbations of the global carbon cycle (Ward et al. 2001; Pálfy et al. 2001; Hesselbo et al. 2002). The end-Triassic is marked by a major mass extinction event (Newell 1963; Raup and Sepkoski 1984; Hallam and Wignall 1997) occurring in coincidence with a

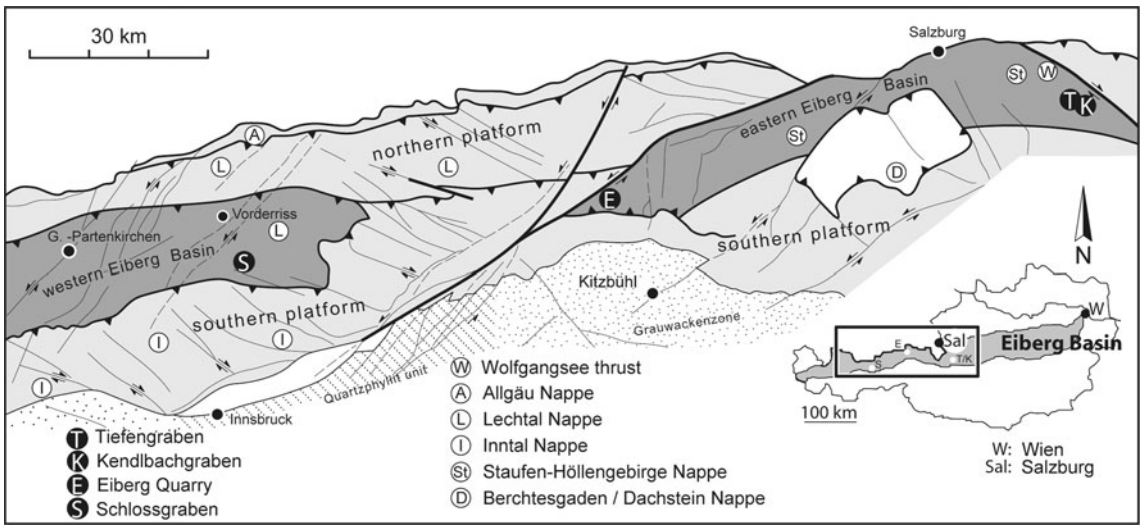

Fig. 1 Tectonic map of the Eiberg Basin, and location of the studied sections, within the western northern Calcareous Alps (modified from Linzer et al. 1995; Hillebrandt and Krystyn 2009)

preeminent negative carbon isotope excursion (Ward et al. 2001; Guex et al. 2004).

While a large consensus exists on the coincidence of the CAMP magmatic activity and the biological crisis (Marzoli et al. 1999, 2004; Schaltegger et al. 2008; Cirilli et al. 2009; Schoene et al. 2010), different interpretations exist regarding the role and effects of the volcanic degassing, which induced very different environmental effects. Carbon dioxide (CO_2) and clathrate melting have been invoked as triggers of a catastrophic greenhouse effect resulting in a carbonate crisis and mass extinction (McElwain et al. 1999; Pálfy et al. 2001; Hesselbo et al. 2002; Hautmann 2004; Galli et al. 2005). On the other hand, Tanner et al. (2001), McHone (2002), Tanner et al. (2004), Guex et al. (2004), and van de Schootbrugge et al. (2009) propose that sulphur dioxide (SO_2) may have induced lower temperatures and acidification as triggers of the main biocalcification crisis and extinction.

The present paper aims to better understand the role of marine biotic productivity during the end-Triassic mass extinction through the synecological change of calcareous benthic and planktonic communities. We focused on the collapse of the carbonate biological pump coinciding with the carbon negative excursion at the end-Triassic. At that time, a large fraction of the calcareous mud in the marginal seas was supplied by calcareous nannofossils (Di Nocera and Scandone 1977; Bellanca et al. 1995). The switch-off of the pelagic carbonate production at the end-Triassic had probably a strong impact on the marine carbonate pump and on the entire carbon cycle. The relationships among surface/carbonate production, bottom oxygen level variations and changes in seawater chemistry were addressed through a multi-proxy study combining micropalaeontological, geochemical and sedimentological analyses in three Austrian sections (Eiberg, Schlossgraben and Tiefengraben), spanning the Triassic/Jurassic transition.

Geological and sedimentological framework

During the Late Triassic, the Northern Calcareous Alps (NCA; Fig. 1) formed a shelf strip along the western Tethyan margin where extensive carbonate platforms developed (Krystyn et al. 2005). By Rhaetian time, prograding of siliciclastic sedimentation and formation of the intraplatform Eiberg Basin as the result of extensional tectonic strongly reduced the carbonate platform area (Oberrhaet limestone; Krystyn et al. 2005; Ruhl et al. 2009). The original geometry and extension of the Eiberg Basin is hard to define because it is tectonically delimited on three sides, except to the southeast where a stratigraphic contact to the adjacent platform is well exposed (Krystyn et al. 2005; Fig. 1).

The three studied sections (Tiefengraben, Eiberg, Schlossgraben) belong to the Eiberg Basin in different palaeogeographical settings (Figs. 1, 2). The Tiefengraben section [47°41′45″N/13°21′00″E] and the section in the Eiberg quarry [47°33′00″N/12°10′07″E] lie within the Osterhorn-Unken Syncline of the eastern part of Eiberg Basin (Fig. 1). Tiefengraben section is located relatively close to the southern Dachstein carbonate platform. Eiberg quarry section is located in a more distal position relative to this carbonate platform, and in a more subsiding area and deep setting of the basin. The Schlossgraben section [47°28′32″N/11°28′55″E] is situated within the Karwendel

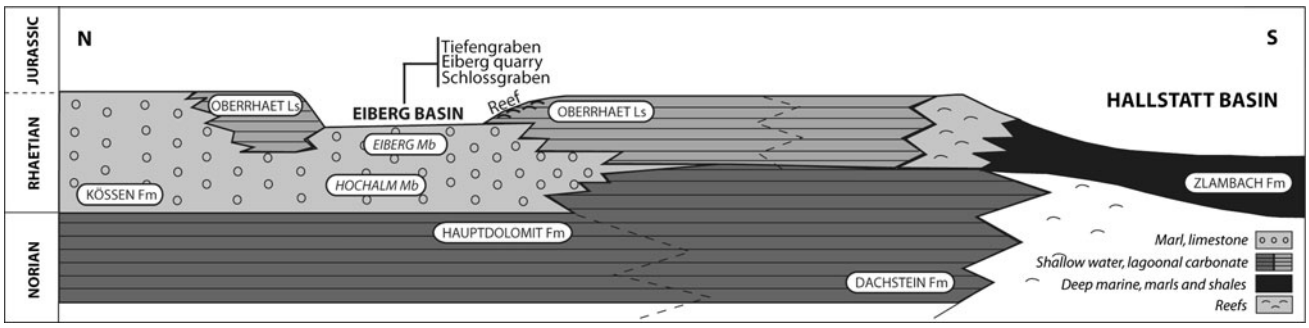

Fig. 2 North-South transect of the Late Norian to Rhaetian facies of the northern Calcareous Alps (modified after Kuerschner et al. 2007) and palaeogeographical setting of the Schlossgraben, Eiberg and Tiefengraben sections within the Eiberg Basin

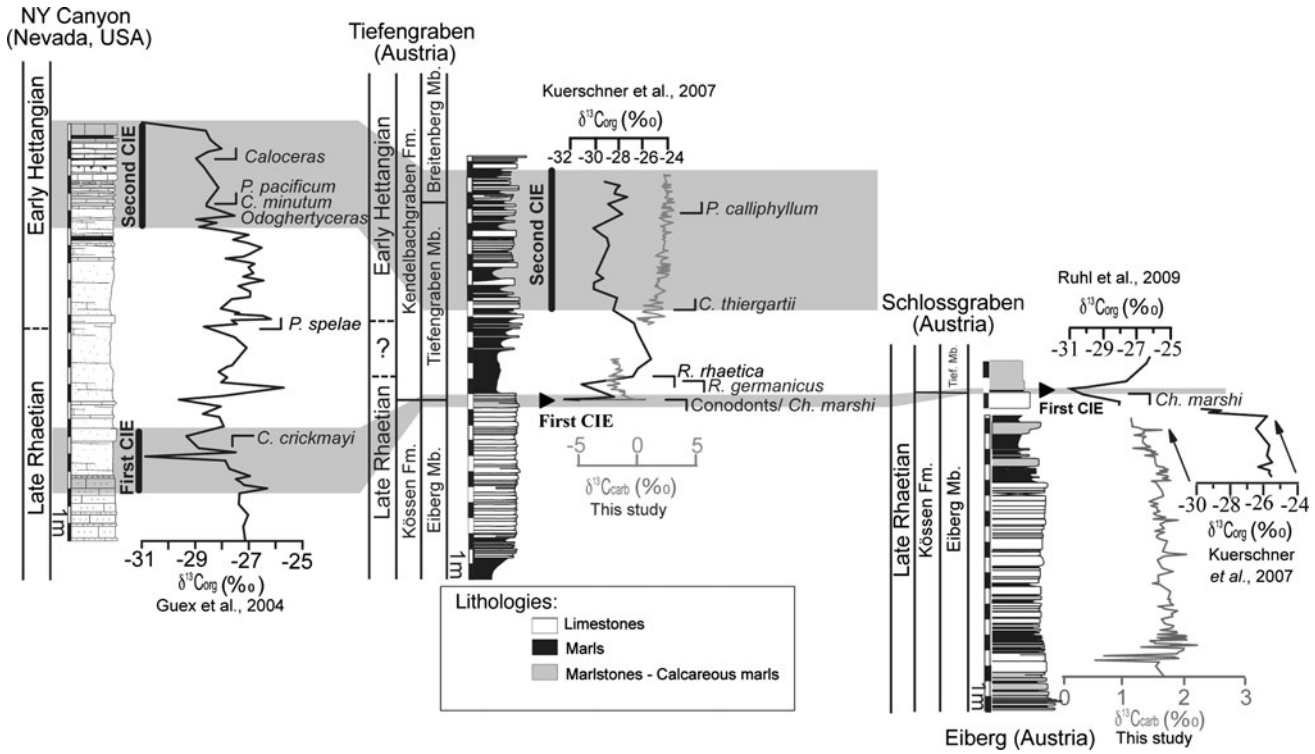

Fig. 3 Integrated bio- and chemostratigraphy and correlation of the T-J boundary between New York Canyon (Nevada, USA; Guex et al. 2004); Tiefengraben, Eiberg and Schlossgraben sections (Northern Calcareous Alps). Tiefengraben δ13Corg profiles are from Kuerschner et al. (2007) and from this study, and those for the Schlossgraben section are from Ruhl et al. (2009), from Kuerschner et al. (2007), and from this study

syncline of the western Eiberg Basin (Fig. 1; Hillebrandt et al. 2007). More detailed lithostratigraphic, palaeogeographical and geological descriptions of the studied sections can be found in Krystyn et al. (2005), Kuerschner et al. (2007), Hillebrandt et al. (2007), Ruhl et al. (2009), and Hillebrandt and Krystyn (2009).

A distinct lithological change from limestones with marlstone intercalations (Eiberg Mb, Kössen Fm) to clayey-marly sediments (Tiefengraben Mb, Kendelbach Fm) defines the sedimentary sequences throughout the Eiberg Basin at the transition from the Triassic to the Jurassic (Fig. 3). This lithological break characterizes a rapid sea-level fall at the end-Triassic that caused a widespread emergence of the platform and surrounding shallow water areas, followed by a slow, long-term sea-level rise that started during the latest Rhaetian and continued through the Hettangian until the Late Sinemurian (Krystyn et al. 2005). However, the Eiberg Basin underwent continuous subsidence during the Late Rhaetian and, as a result, deposition was less affected by the end-Triassic sea-level drop, especially in deeper parts of the basin (e.g., Eiberg and Schlossgraben) where fully marine conditions

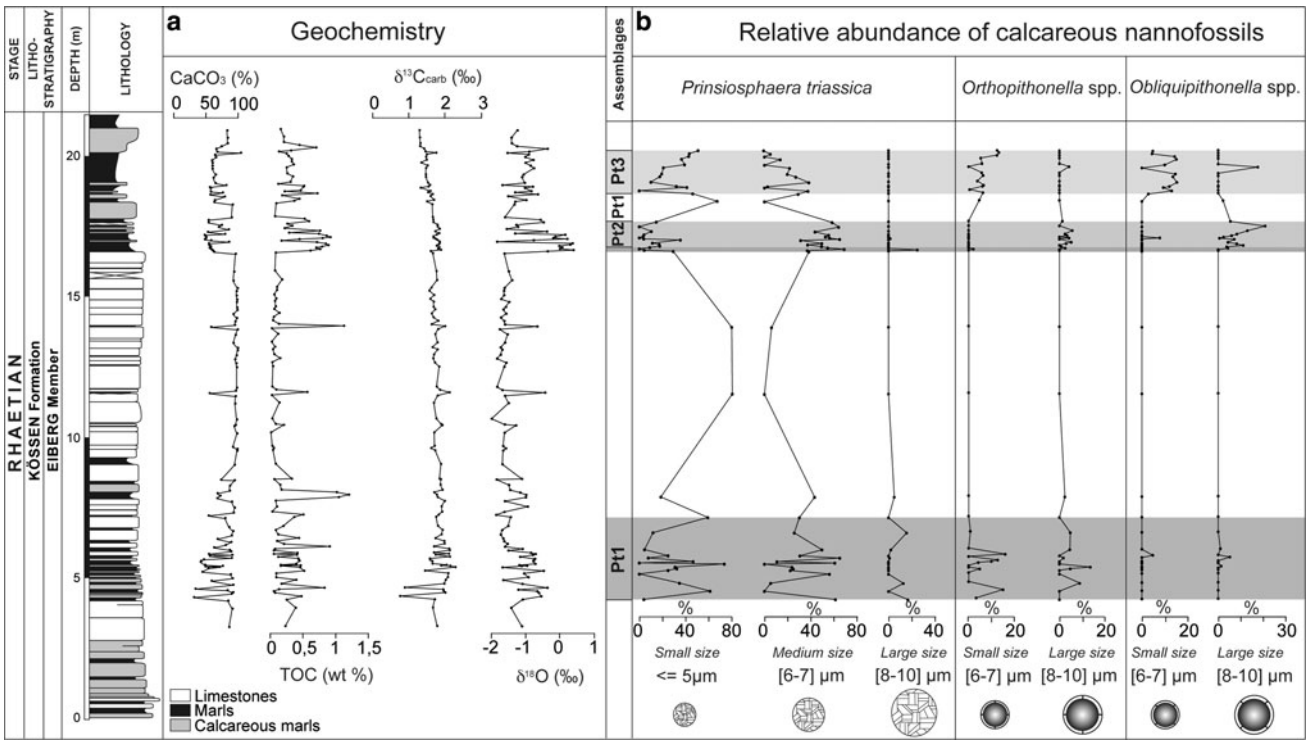

Fig. 4 Eiberg section. **a** High-resolution geochemistry. Carbonate, total organic carbon (TOC), organic carbon isotope ($\delta^{13}C_{org}$), and C and O isotope composition of carbonate ($\delta^{13}C_{carb}$, and $\delta^{18}O$). **b** Relative abundance (in %) of small (<5 µm), medium-sized (6–7 µm) and large (8–10 µm) *P. triassica* and calcareous cysts throughout the section

prevailed continuously, as attested by fauna reported by Hillebrandt and Krystyn (2009). In the Eiberg basin the carbonate and marly content of the Kössen Fm depends on a more distal or proximal position with respect to the carbonate platforms (Kuerschner et al. 2007).

In a distal setting such as the Eiberg quarry section, the upper part of the Kössen Fm is characterized by thin (5–10 cm) calcareous marl-marl alternation grading into a ~10 m interval of well-bedded (20–40 cm) micritic limestones (Figs. 4, 5, 6). In the uppermost part of the studied section a gradual transition to the Tiefengraben Mb is represented by marl and micritic limestone alternations. The Schlossgraben section (Fig. 7) provides a more complete record of the transition between the topmost Kössen Fm and the Kendelbach Fm. The micritic "T-bed" of the Eiberg Mb is followed by 50 cm thick grey-brown marls of the lowermost part of the Tiefengraben Mb, the first 2–3 cm of which are very rich in organic matter (black-shale level). Therefore, the composite record of the Eiberg and Schlossgraben sections allows constraining the Tr-J transition in a completely marine environment. In the proximal areas relative to carbonate plateform, such as Tiefengraben, the upper part of Kössen Fm is much more calcareous and thickly bedded (Figs. 8, 9) and the contact with the overlying Tiefengraben Mb is very sharp. The lowermost part of the Tiefengraben Mb is characterized by a 3 m thick, grey clayey-marly interval (Grenzmergel), followed by marl-micritic limestone alternations upwards in the section. Palaeontological and palynological studies show that during the latest Triassic, the palaeoenvironment at Tiefengraben shifted from outer to inner-shelf, with very shallow-water and brackish conditions corresponding to the deposition of the lower part of the Tiefengraben Mb (Kuss 1983; Golebiowski 1990; Kuerschner et al. 2007).

Integrated stratigraphic correlations and position of the Tr-J boundary

The position of the Tr-J boundary in the NCA within the Eiberg Basin has been the subject of a variety of interpretations (Kuerschner et al. 2007 and references in there; Hillebrandt and Urlichs 2008; Ruhl et al. 2009; Bonis et al. 2009; Hillebrandt and Krystyn 2009).

In the present paper, we follow the Tr-J boundary definition based on the first occurrence (FO) of *Psiloceras spelae,* the earliest Jurassic psiloceratid occurring at New York Canyon, USA (Guex et al. 2004). In this section, the high-resolution ammonite biostratigraphy allows to calibrate the $\delta^{13}C_{org}$ curve. The beginning of the first negative carbon isotope excursion (CIE) is roughly located at the top of the crickmayi Zone (Rhaetian), which is correlated with

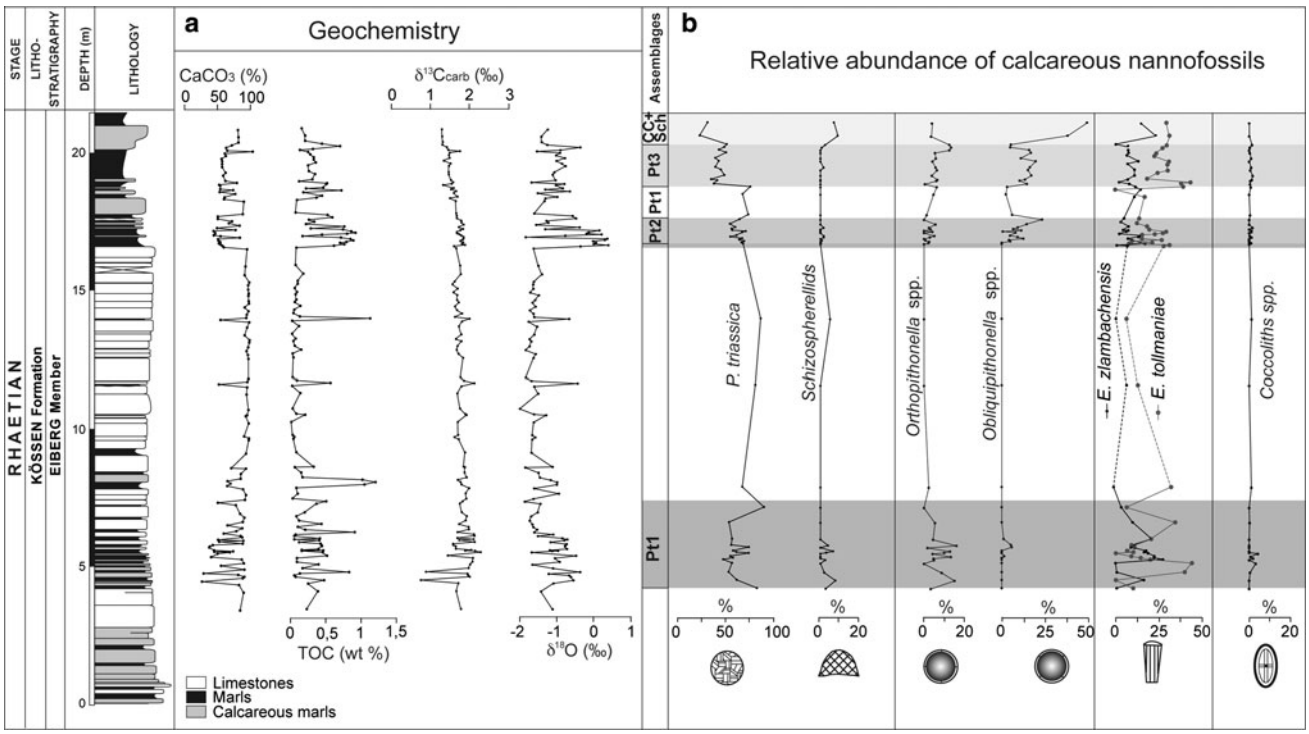

Fig. 5 Eiberg section. **a** High-resolution Geochemistry. Carbonate, total organic carbon (TOC), organic carbon isotope ($\delta^{13}C_{org}$), and C and O isotopic composition of carbonate ($\delta^{13}C_{carb}$, and $\delta^{18}O$). **b** Relative abundance (in %) of calcareous nannofossils. Calcareous nannofossil assemblages as in Fig. 4

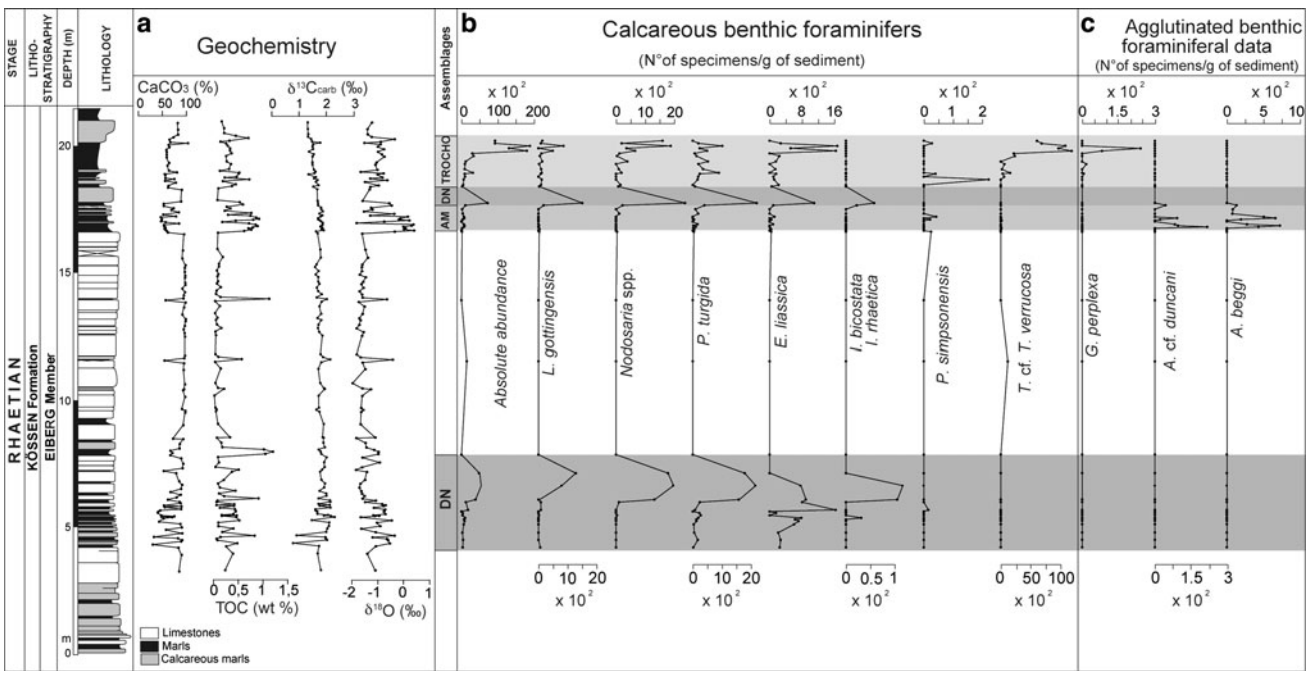

Fig. 6 Eiberg section. **a** High-resolution geochemical data. Carbonate, total organic carbon (TOC), organic carbon isotope ($\delta^{13}C_{org}$), and C and O isotopic composition of carbonate ($\delta^{13}C_{carb}$ and $\delta^{18}O$). **b** Abundance of calcareous benthic foraminifera expressed as number of specimens per gram of sediment. **c** Abundance of agglutinated benthic foraminifera expressed as number of specimens per gram of sediment

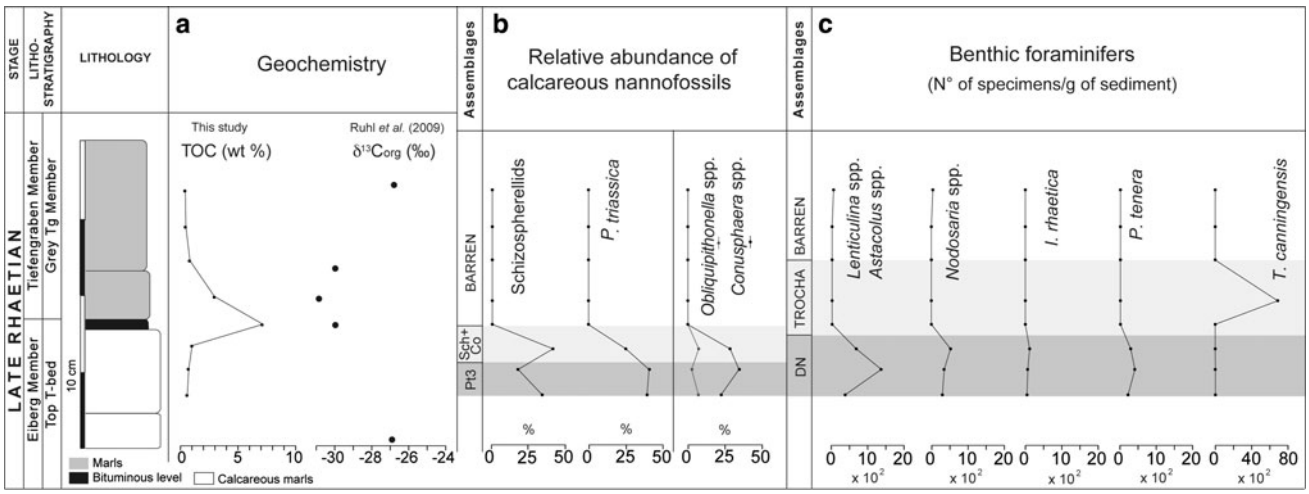

Fig. 7 Schlossgraben section. **a** Geochemistry. Total organic carbon (TOC). Organic carbon isotopic composition ($\delta^{13}C_{org}$) from the Schlossgraben and Kuhjoch sections (data from Ruhl et al. 2009). **b** Relative abundance (in %) of calcareous nannofossils. **c** Abundance of benthic foraminifera expressed as number of specimens per gram of sediment

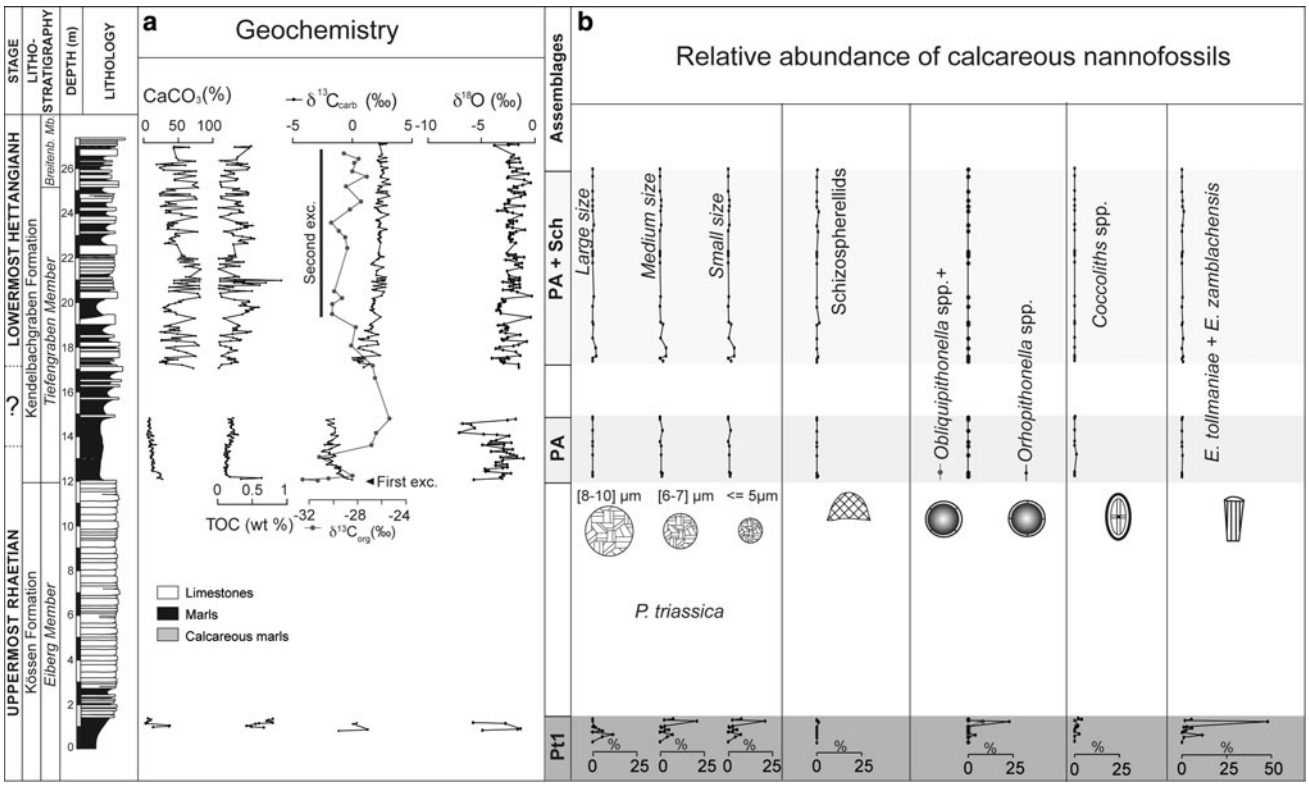

Fig. 8 Tiefengraben section. **a** High-resolution geochemistry. Carbonate, total organic carbon (TOC), organic carbon isotope ($\delta^{13}C_{org}$), and C and O isotopic composition of carbonate ($\delta^{13}C_{carb}$ and $\delta^{18}O$). **b** Relative abundance (in %) of calcareous nannofossils

the upper part of the marshi Zone in Tethyan sequences (e.g., Eiberg and Schlossgraben; Fig. 3). The FO of *P. spelae* occurs within the positive CIE between the two negative CIEs. *P. spelae* was found in the Eiberg basin (Hillebrandt and Krystyn 2009), but not at Tiefengraben. However, if we correlate the positive CIE recorded at this locality (Kuerschner et al. 2007) with that of New York Canyon, the Tr-J boundary in this section lies approximately 13–17 m above the base of Tiefengraben section (Fig. 3), slightly below the position based on palynological data given by Kuerschner et al. (2007), Ruhl et al. (2009) and by Bonis et al. (2009). The *calliphyllum* Beds located

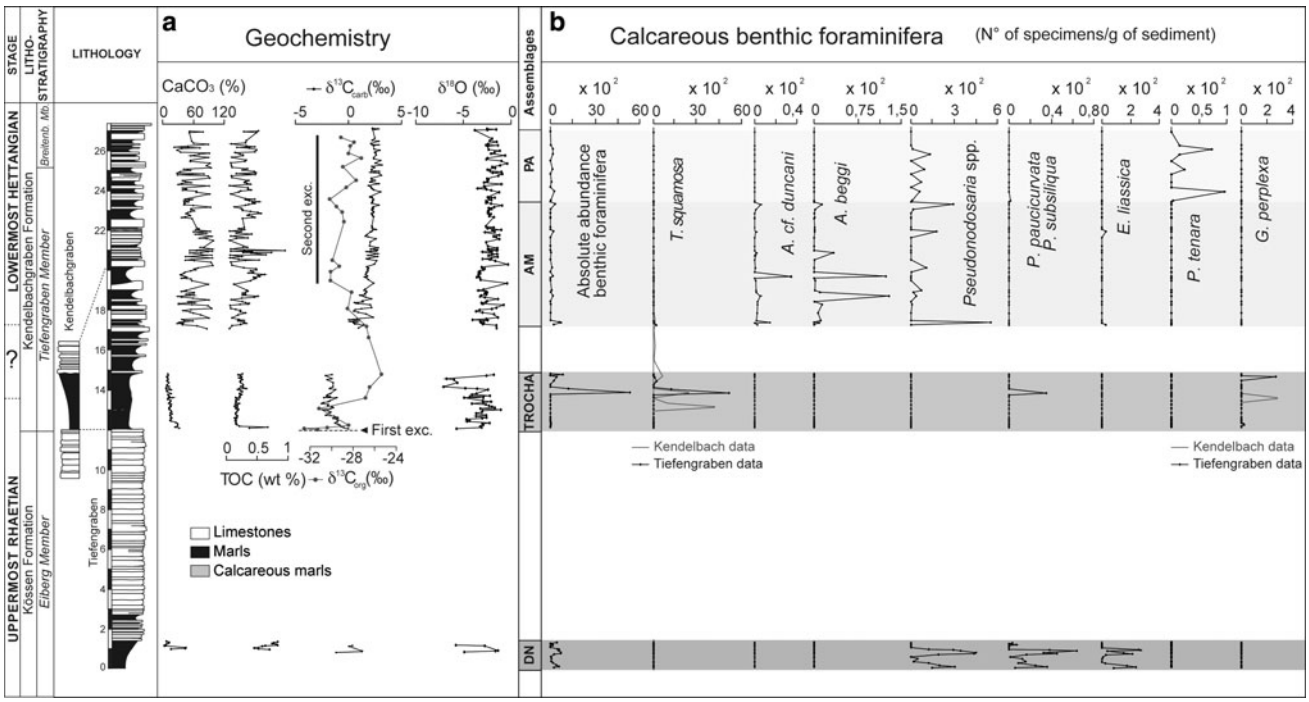

Fig. 9 Tiefengraben and Kendelbachgraben sections. **a** High-resolution geochemical data from Tiefengraben. Carbonate, total organic carbon (TOC), and C and O isotopic composition of carbonate ($\delta^{13}C_{carb}$ and $\delta^{18}O$). **b** Abundance of benthic foraminifera expressed as number of specimens per gram of sediment

within the second negative CIE at Tiefengraben, are correlated with the upper *pacificum* to lower *polymorphum* Beds at New York Canyon.

Materials and methods

Calcareous nannofossils

Calcareous nannofossils were examined under both SEM and optical microscopes. A total of 141 smear slides were prepared for nannofossils study according to standard preparation techniques (Bown and Young 1998). Samples from Eiberg, Schlossgraben and Tiefengraben sections were taken from the marlstone and calcareous marlstone beds, and prepared as homogeneously as possible, in order to maintain comparable particle density in all slides. Nannofossils were observed in smear slides under a polarising-light microscope (Zeiss Axioplan II), at a magnification of $\times$1,575. At least 300 specimens were counted in each smear slide to quantify the relative abundance of taxa and to analyse the stratigraphic changes in assemblage composition. Due to the scarcity of nannofossils in some samples of the Tiefengraben section (from 17 m to the top), $<$300 specimens were counted. Almost all specimens were identified at the species level following the taxonomic definitions of Janofske (1987, 1992), Bown (1987) and Bralower et al. (1991). The diameter of *P. triassica, Obliquipithonella* sp. and *Orthopithonella* sp. (calcareous cysts) was measured on digital images using a CCD-video camera mounted on a Zeiss optical microscope with an accuracy of $\pm$0.1 µm. We distinguished three size-classes for *P. triassica* and two for calcareous cysts (Figs. 4b, 8b).

Benthic foraminifera

The samples used for calcareous nannofossil analysis were also used for benthic foraminifera analysis. For the shaly-marly interval at the base of Tiefengraben Member (Grenzmergel), a complementary sampling was done in the section of Kendelbach, located very close to the Tiefengraben section (Fig. 1). 300 g of dry sediment was kept in Desogen (alchyldimethyl-benzylamin chlorure) for 48 h to flocculate the argillaceous fraction. Material larger than 63 µm was sieved, washed and dried at 50°C. After sieving residues through 1 mm, 500, 250, 125 and 63 µm meshes, foraminifera were picked up, identified according to the classification established by Loeblich and Tappan (1987) and counted under a binocular microscope. For the most representative genera, the absolute abundance (i.e., the number of foraminifera per gram of dried sediment) was calculated. Because of the very small quantity of benthic

foraminifera in some samples of the upper part of the Tiefengraben section (from 17 m to the top), these results must be interpreted with some caution.

Total organic carbon and carbonate analysis

Two-hundred and four samples from Tiefengraben, eight samples from Schlossgraben and 130 samples from Eiberg were crushed into a fine powder. Analyses were performed on a Rock–Eval 6 device (IFP, France). The device was calibrated with the IFP standard 160000, and the methodology described for bulk rocks in Behar et al. (2001) is applied. Type of organic matter (OM) was determined using hydrogen and oxygen indexes. T_{max} values provide information on the thermal maturation stage of the organic matter. Rock–Eval analyses provide both mineral and organic carbon content records (respectively $CaCO_3$ weight% and TOC weight%, total organic carbon).

Inorganic carbon and oxygen isotope analysis

For carbon and oxygen isotope analyses of the carbonates, 188 samples from Tiefengraben and 130 samples from Eiberg were processed at the SSMIM (Muséum National d'Histoire Naturelle of Paris, France). The $\delta^{13}C_{carb}$ and $\delta^{18}O$ values were measured in a "Delta V Advantage" (Thermofischer Scientific) isotope ratio gas mass spectrometer directly coupled to a "Kiel IV" automatic carbonate preparation device (reaction at 70°C under vacuum) and calibrated via NIST 19 to the VPDB (Vienna Pee Dee Belemnite) scale. The overall precision of the measurement was better than 0.03 and 0.04‰ for carbon and oxygen, respectively. Reproducibility of replicated standards is typically better than 0.1‰ for $\delta^{13}C_{carb}$ and $\delta^{18}O$.

Diagenesis

Geochemical signal

The Tiefengraben, Schlossgraben and Eiberg sections contain organic matter (OM) without any evidence for thermal maturation ($T_{max} = 430$°C), excluding a significant burial or alteration through thermal diagenesis. Therefore, we interpret this OM as reflecting primary environmental conditions.

At Eiberg, the $\delta^{13}C_{carb}$ and $\delta^{18}O$ values show a range of about 0.8 to 2.3‰ and 0.3 to −1.9‰ respectively (Figs. 4a, 10a), indicating an isotopic signature that has not been strongly affected by burial diagenesis. Moreover, the non-linear covariation ($r^2 = 0.02$) between $\delta^{13}C_{carb}$ vs. $\delta^{18}O$ values can be also an index of weak diagenetical alteration (Fig. 10a). On the other hand, an apparent correlation is

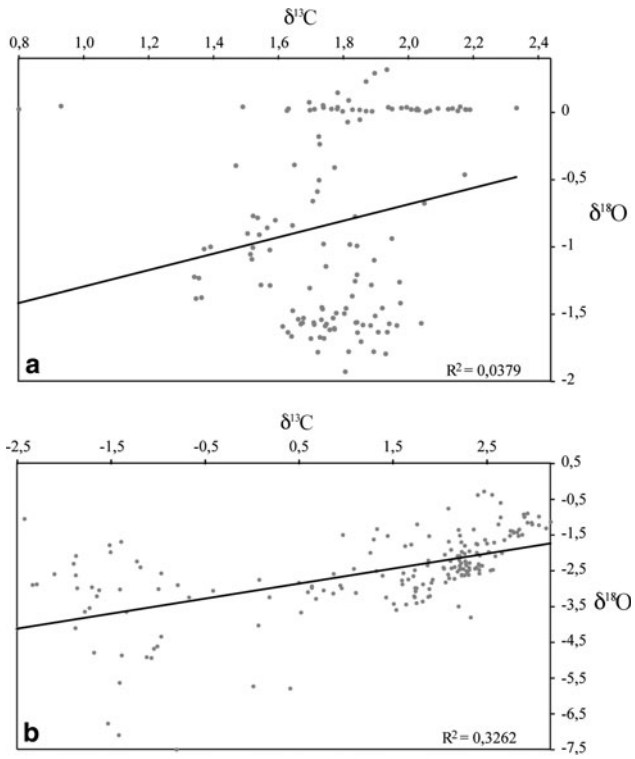

Fig. 10 Plots of $\delta^{13}C_{carb}$ against $\delta^{18}O$ for samples of the Eiberg section (**a**) and Tiefengraben section (**b**)

observed between the $\delta^{18}O$ and $CaCO_3$ (Fig. 4a). Lighter $\delta^{18}O$ values seem to characterise limestone-beds, whereas heavier $\delta^{18}O$ values seem more closely related to marly interbeds. Limestone-beds are more likely to be diagenetically affected than marly beds, as a consequence of the contrast in permeability, and thus, diagenesis has certainly amplified the $\delta^{18}O$ gradient between limestones and marlstones. However, the mudstone-wackestone textures of limestones imply that the water–rock ratio was very low, promoting the conservation, at least in part, of primary signals (Marshall 1992). Consequently, despite the preservation limits described above, it is still possible to interpret the general trend of $\delta^{13}C_{carb}$ and $\delta^{18}O$ variations, as a palaeoenvironmental signal.

At Tiefengraben, the carbonate $\delta^{13}C_{carb}$ and $\delta^{18}O$ records have suffered a major diagenetic impact with respect to the Eiberg section. The $\delta^{18}O$ measurements are quite scattered with a wide range of values (between 0 and −8‰; Fig. 8a), sometimes with very low values (<−5‰). Also, the $\delta^{13}C_{carb}$ curve presents a wide range of values (between 0 and +3‰), although they stay positive and could be less altered than those of the $\delta^{18}O$ values. A good correlation of $\delta^{13}C_{carb}$ vs. $\delta^{18}O$ values is also observed ($r^2 = 0.4$; Fig. 10b). This linear correlation and the very light values of $\delta^{18}O$ might be related to meteoric diagenesis (Marshall 1992). The covariance between the $\delta^{13}C_{carb}$ and

$\delta^{18}O$ values could also be explained by an early diagenesis depositional model, driven by salinity variations (Fig. 10b). Light $\delta^{18}O$ and $\delta^{13}C_{carb}$ values may reflect a balance between fluvial (isotopically light $\delta^{18}O$ and $\delta^{13}C_{carb}$ values) and marine influxes (Marshall 1992). During the phases of lowered salinity, because of lowered pH, carbonate production was hampered and carbonate dissolution-re-precipitation reactions occurred, while during marine influxes phases (heavy $\delta^{13}C_{carb}$ and $\delta^{18}O$ values) major carbonate production and preservation was possible. As such, this interpretation agrees with the palaeontological and sedimentological interpretations of shallow, brackish water environment for a great part of Tiefengraben Mb (Kuerschner et al. 2007). For the Tiefengraben section therefore, we cannot exclude that early diagenesis linked to salinity variations might have amplified isotopic variations, and we dismissed interpretation of the temperature trend, due to very scattered fluctuations and very negative values of $\delta^{18}O$.

Biotic signal

Dissolution and overgrowth affect the preservation of the biological signal making it more difficult to interpret the records of the Tr-J transition with confidence. Both optical and SEM analyses were used to estimate of the state of calcareous nannofossil preservation. The preservation state although moderate to poor, does not vary significantly along one and the same section. Nannofossil assemblages from Eiberg and Schlossgraben show an overall moderate preservation compared to Tiefengraben where preservation is generally poor. Pervasive re-crystallization affecting taxa such as "Schizosphaerellids", *Orthopithonella* spp. and *Obliquipithonella* spp. was frequently observed during SEM analysis (Fig. 11), although these taxa can still be identified with an optical microscope due to their specific optical properties. Bralower et al. (1991) documented four preservation stages with respect to the amount of etching affecting the structure of *P. triassica*. We did distinguish the four stages within the assemblages, although we did not observe any direct relation between the amount of etching and poor preservation, as proposed by these authors. Poorly-preserved calcareous nannofossils are associated with calcite rhombs, probably due to in situ dissolution and re-precipitation during diagenesis. These diagenetic overprints may affect the quantitative estimates and for this reason only the major trends and shifts within the assemblages were taken into account for the palaeoenvironmental interpretations.

In general, the calcitic foraminiferal tests are moderately-preserved and filled in with secondary calcite. SEM observations reveal re-crystallization and overgrowth in their walls (Fig. 12f–w, z). Aragonitic tests (e.g., *Trocholina*) are poorly preserved, display traces of dissolution and/or are severely re-crystallized (Fig. 12a). We found agglutinated benthic foraminifera (Fig. 12b–e, x, y) to be highly dominant or exclusive in the assemblages of several stratigraphic levels (Figs. 6c, 7c, 9b) indicating lowered pH conditions (Hemleben et al. 1990). The main question is whether or not these low pH conditions correspond to primary environmental changes, or if they are related to diagenetic processes. Preferential dissolution of calcareous foraminifera enhancing agglutinated foraminifera abundance could be linked to secondary diagenetic processes (Scott et al. 1983). However, primary oceanic acidification events could also be a possible reason. In the fossil record, the distinction between these last two factors can be very subtle, and therefore difficult to assess. At Eiberg in the uppermost Rhaetian, peaks in the abundance of fine agglutinated *Ammobaculites* spp. and *Ammomarginulina* spp. are correlated with high $\delta^{18}O$ values (Fig. 6), showing that diagenetic dissolution impact is absent or minimal. In general, a secondary diagenesis impact results in a decreasing $\delta^{18}O$ signature (Marshall 1992). At Tiefengraben, Kendelbach and Schlossgraben, peaks in the abundance of the agglutinated foraminifera *Glomospira perplexa, Trochammina squamosa* and *T. canningensis* (Fig. 12b–e) can be observed in the uppermost Triassic (Figs. 7c, 8, 9b). In some levels we found them associated with few hyaline foraminifera, showing obvious traces of dissolution. Therefore, we cannot ignore that severe dissolution possibly has affected the preservation of hyaline foraminifera, and thereby artificially enhancing the *T. squamosa* and *T. canningensis* occurrences (Scott et al. 1983). Consequently, the abundances of *T. squamosa* and *T. canningensis* must be interpreted cautiously. However, this dissolution may also reflect primary low pH environmental conditions (acidification event). Several reasons support such a hypothesis:

(1) In coincidence with the *T. squamosa* peaks, $\delta^{18}O$ values are not significantly more negative when compared with other levels, where exclusively hyaline taxa are present (Fig. 9b). This means that high abundance of *T. squamosa* does not seem to be associated with levels of stronger secondary diagenetic impact.
(2) The occurrence of *T. squamosa* and *T. canningensis* seems to be confined within a specific stratigraphic interval (just after the first negative $\delta^{13}C$ shift). We do not observe any occurrence below or above this interval. Their occurrence seems, therefore, to be unequivocally associated to peculiar environmental conditions.
(3) We observed a typical succession of agglutinated foraminifera assemblages (from *Trochammina* to coarse agglutinated *Ammobaculites-Ammomarginulina* assemblage) correlated with variations of carbon

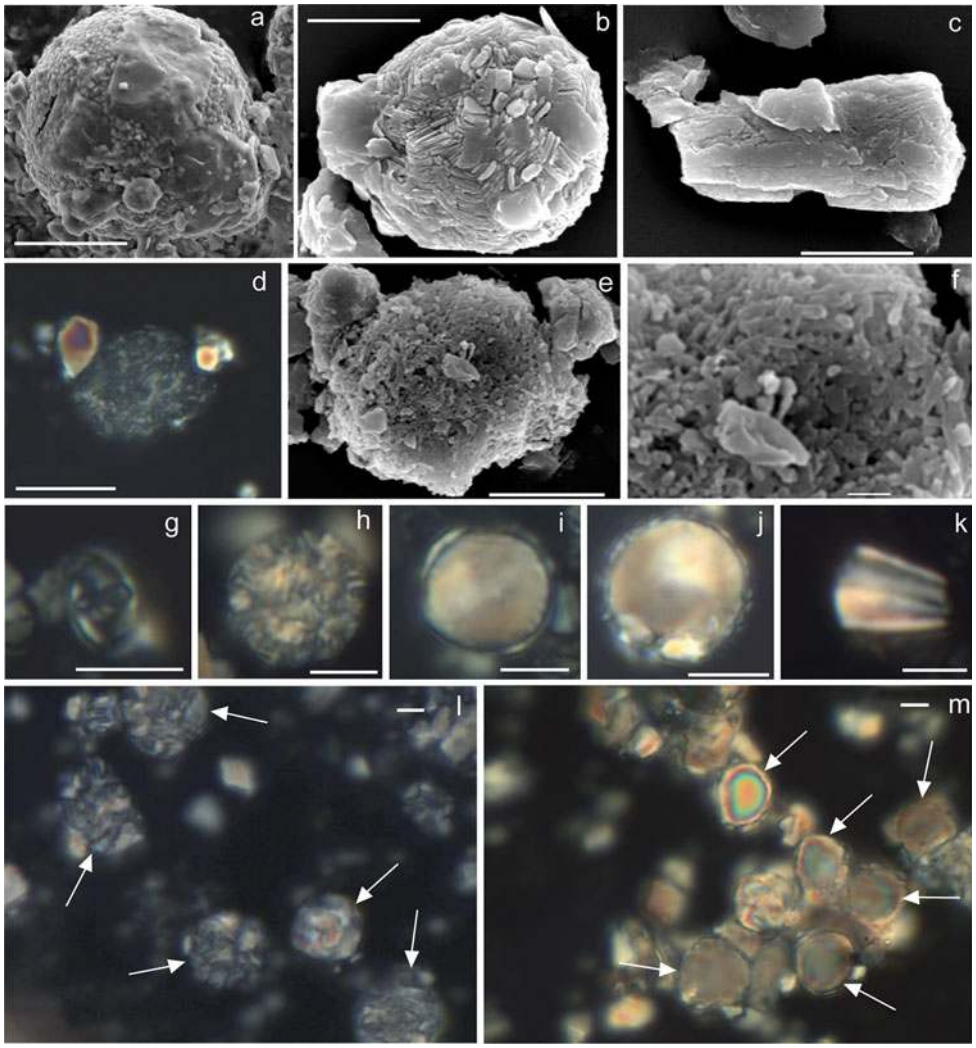

Fig. 11 Calcareous nannofossils. **a** *Orthopithonella geometrica* (Jafar, 1983) Janofske, 1987. Sample EB364, Eiberg section, Late Rhaetian, SEM picture, *scale bar* = 5 µm. **b** *Prinsiosphaera triassica* Jafar, 1983. Sample TGR17, Tiefengraben section, Late Rhaetian, SEM picture, *scale bar* = 5 µm. **c** *Eoconusphaera zlambachensis* (Moshokovitz, 1982) Kristan-Tollmann, 1988a. Sample EB361, Eiberg section, Late Rhaetian, SEM, *Scale bar* = 5 µm. **d–f** *Schizosphaerella* sp. Sample HC1, Schlossgraben section, Late Rhaetian. **d** LM (Light microscope), *scale bar* = 10 µm. **e** SEM (Scanning electron microscope) picture, *scale bar* = 10 µm. **f** Detail of (**e**) showing the structure of the wall, *scale bar* = 1 µm. **g** *Archeozygodiscus koessensis* Bown, 1985. Sample TGR18rh, Tiefengraben section, Late Rhaetian, LM, *Scale bar* = 5 µm. **h** *Prinsiosphaera triassica* Jafar, 1983. Sample TGR9rh, Tiefengraben section, Late Rhaetian, LM, *scale bar* = 5 µm. **i** *Orthopithonella geometrica* (Jafar, 1983) Janofske, 1987. Sample EB361, Eiberg section, Late Rhaetian, LM, *scale bar* = 1 µm. **j** *Obliquipithonella rhombica* Janofske, 1987. Sample EB392, Eiberg section, Late Rhaetian, LM, *scale bar* = 5 µm. **k** *Eoconusphaera zlambachensis* (Moshokovitz 1982) Kristan-Tollmann, 1988a. Sample TGR17rh, Tiefengraben section, Rhaetian, LM, *scale bar* = 1 µm. **l** Detail of "*P. triassica assemblage with large forms*" with several large *P. triassica*. Sample EB300, Eiberg section, Late Rhaetian. LM, *scale bar* = 10 µm. **m** Detail of "*P. triassica assemblage with small forms*" with several calcareous cysts. Sample EB350, Eiberg section, latest Rhaetian. LM, *scale bar* = 5 µm

isotopes and TOC (Fig. 9). This biotic pattern cannot be explained solely by diagenetic processes. On the contrary, it also seems to reflect environmental variations. Moreover, in conjunction with the second negative CIE, agglutinated *Ammobaculites* cf. *duncani* and *Ammomarginulina beggi* are associated with very thin (<125 µm) hyaline foraminifera (*Pseudonodosaria limpida*), thereby ruling out a strong impact of diagenetic dissolution for this assemblage.

Palaeoenvironmental reconstruction

Characterisation of organic matter

Eiberg, Schlossgraben and Tiefengraben results (Fig. 13) display OM of Type III, particularly the bituminous level at Schlossgraben coinciding with the first $\delta^{13}C_{org}$ negative shift (7% of TOC; Fig. 7). Only a few samples at the base of the thick calcareous interval at Eiberg are characterized

by marine OM of Type II (Fig. 13). We could not discriminate if this Type III OM is fully continental or originally marine OM that suffered alteration. However, huge terrestrial palynomorph concentrations (mainly conifer Cheirolepidiaceae pollen) were documented in the coeval bituminous level of the nearby Hochalpgraben and Kuhjoch sections (Bonis et al. 2009). This terrestrial influence could reflect the limited surface productivity during the end-Triassic regression in conjunction with the negative carbon isotope shift. Similarly, Kuerschner et al. (2007) noticed a clear increase of terrestrial versus marine palynomorphs during the end-Triassic interval in Tiefengraben and Eiberg sections.

Carbon and oxygen stable isotopes

Interpreting the evolution of $\delta^{13}C_{carb}$ and $\delta^{18}O$ signatures along the Eiberg section is difficult. In the lower part of the studied section (from the base to 6.3 m), short-term fluctuations of $\delta^{18}O$ seem to follow the marly-limestone alternations (Fig. 4a). Beyond the diagenetic impact discussed above (see Sect. "Geochemical signal"), one may ask whether yes or no these fluctuations are also driven by cyclic temperature and/or salinity changes. The short-term, lighter $\delta^{13}C_{carb}$ values correlate with increased TOC values, and this might be related to partial recycling of OM. Further studies are needed to confirm whether these $\delta^{13}C_{carb}$ and $\delta^{18}O$ short-term variations are responding to cyclic variations of sea-level changes, or to other factors. In the middle to upper part of the section (6.3–16.6 m, represented by the thick calcareous interval), both $\delta^{13}C_{carb}$ and $\delta^{18}O$ values tend to be more stable, with the exception of two higher $\delta^{18}O$ points, correlating with higher TOC and lower $CaCO_3$ values (Fig. 4a). In the uppermost part of the section (from 16.5 m upwards), both $\delta^{13}C_{carb}$ and $\delta^{18}O$ show a more distinct pattern with respect to "background" fluctuations. A gradual decreasing trend of $\delta^{13}C_{carb}$ (from 2 to 1‰) is clearly observed, which could correspond to the pre-excursion interval, just before the sharp negative shift, as indicated in the $\delta^{13}C_{org}$ curve of Kuerschner et al. (2007). In contrast with the gradual variation of the $\delta^{13}C_{carb}$ signal, the fluctuations of $\delta^{18}O$ values appear more abrupt and a major break at 16.5 m is underlined by a sharp positive shift of the $\delta^{18}O$ values (from −1.58 to 0.32‰; Fig. 4). This abruptness could partially have been accentuated by a diagenetical overprinting, as discussed above (see Sect. "Geochemical signal"). However, this major positive $\delta^{18}O$ shift has a clearly different amplitude and is associated with peculiar micropalaeontological features with respect to the other positive fluctuations recorded along the section (Figs. 4, 5, 6). It might be related to a temperature decrease (i.e., cooling pulse) and/or seawater chemistry change. As a matter of facts, the oxygen isotope fractionation between calcium carbonate and seawater does not only depend on temperature, but also on the CO_3^{2-} concentration or the pH (Zeebe and Westbroek 2003). This interpretation is in full agreement with our micropalaeontological data: the occurrence of agglutinated benthic foraminifera is related to low pH environments, whereas the demise of *P. triassica* could indicate reduced $CaCO_3$ Ω (see Sect. "Biotic signal").

At Tiefengraben, besides brackish conditions and poor preservation, (see Sect. "Geochemical signal"), some more general trends can still be detected in the $\delta^{13}C_{carb}$ curve when compared with the $\delta^{13}C_{org}$ curve of Kuerschner et al. (2007) (Fig. 8a). The $\delta^{13}C_{org}$ curve shows two distinct negative CIEs during the uppermost Rhaetian and lower Hettangian respectively, separated by a positive CIE close to the Tr-J boundary. Very low $\delta^{13}C_{carb}$ values coincide in part with the uppermost Rhaetian negative $\delta^{13}C_{org}$ CIE (Fig. 8a). This negative excursion observed both in the organic and inorganic carbon record has been observed in several sections, from different environmental settings, and may indicate a perturbation of the global carbon cycle in coincidence with the end-Triassic mass extinction (McRoberts et al. 1997; Ward et al. 2001; Pálfy et al. 2001; Guex et al. 2004; Galli et al. 2005; Ruhl et al. 2009). Coinciding with the second negative excursion of $\delta^{13}C_{org}$, the $\delta^{13}C_{carb}$ values remain relatively high (Fig. 8a). This negative correlation between the $\delta^{13}C_{carb}$ and $\delta^{13}C_{org}$ curves in the Early Hettangian is not just a local feature because it was also observed in the Blue Lias Formation at Doniford (SW England, Clémence et al. 2010).

Micropalaeontological data

We defined a succession of calcareous nannofossil and benthic foraminiferal assemblages characterized by dominant and palaeoecologically important taxa (Tables 1, 2). These assemblages document significant quantitative and qualitative changes that occurred at the Tr-J transition, as shown in Figs. 4, 5, 6 for Eiberg, in Fig. 7 for Schlossgraben and in Figs. 8 and 9 for Tiefengraben.

Palaeoecology of Tr-J benthic foraminifera

The stratigraphic distribution of the benthic foraminiferal assemblages reflects the environmental changes driven by sea-level fluctuations, food supply and oxygen level, in agreement with previously published sedimentological and palaeontological data (Golebiowski 1990; Kuerschner et al. 2007, see Sect. "Geological and sedimentological framework").

Within the marlstone intercalations of the Eiberg Mb at the Eiberg, Schlossgraben and Tiefengraben sections, abundant and diversified Nodosariidae (Figs. 6b, 7c, 9b)

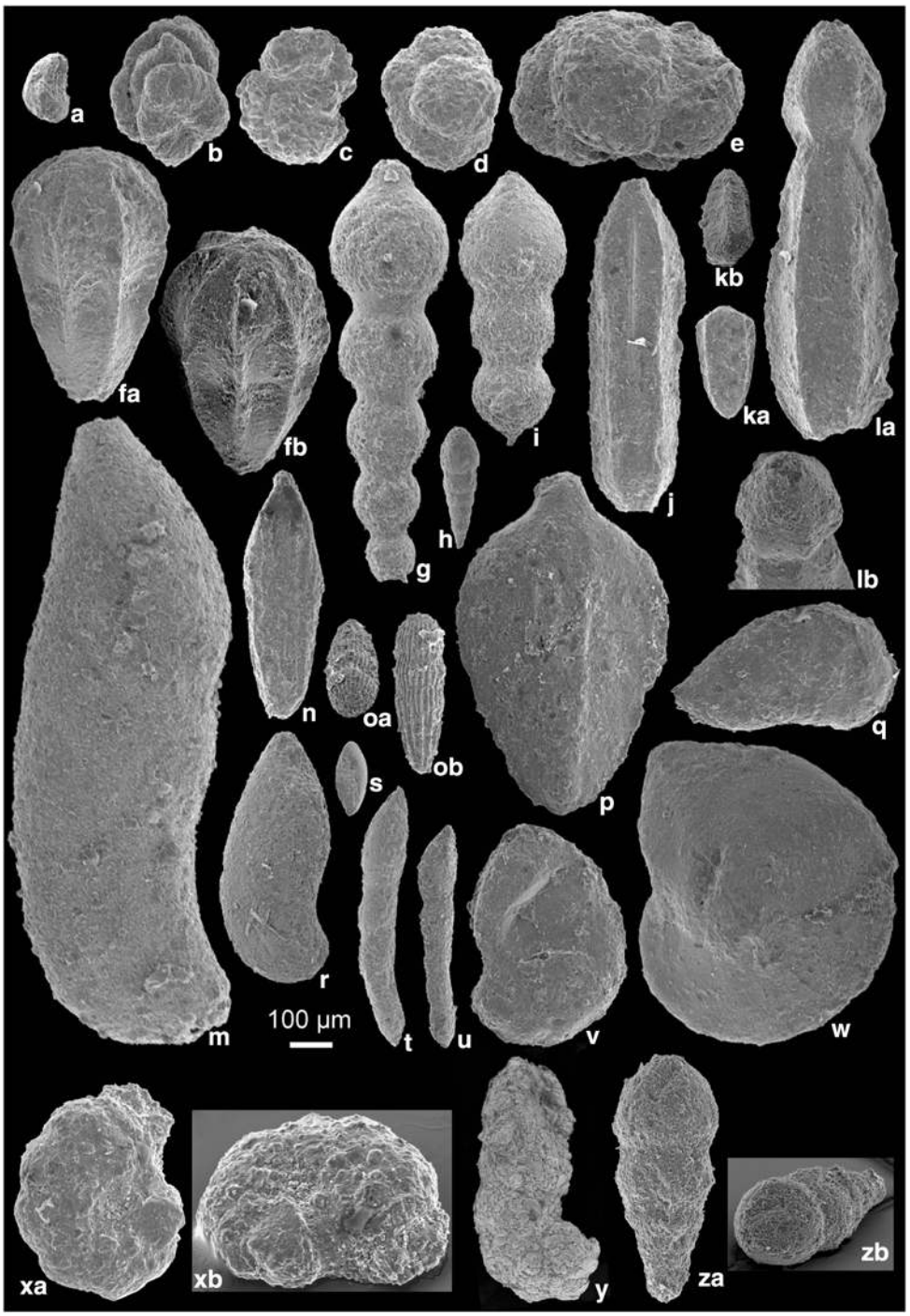

indicate open sea and outer shelf conditions (>50 to around 200 m) with normal marine salinity (Jenkins and Murray 1989). In the same levels, the presence of ammonites and high proportions of marine palynomorphs also support this interpretation (Kuerschner et al. 2007). Abundant and diversified Nodosariidae (Figs. 6b, 7c, 9b) are adapted to well-oxygenated microhabitats (ranging from epifaunal to deep infaunal), and with active deposit-feeder and grazing feeding strategies (Reolid et al. 2008), as confirmed by positive $\delta^{13}C_{carb}$ values and a low OM content (Figs. 6, 7, 9). According to Jorissen et al. (1995) and Gooday (2003), such mixed assemblages may well have existed under mesotrophic conditions (availability of "high quality" labile organic matter), and high levels of dissolved oxygen (Gräfe 2005). This is consistent with the presence of common bioturbations, as well as a rich and diversified macrofauna recorded in this stratigraphic interval (Golebiowski 1990).

◀ **Fig. 12** Selected benthic foraminifera, all *scale bar* = 100 μm. **a** *Trocholina* cf. *T. verrucosa* KRISTAN, 1957. Eiberg section, EB357, Uppermost Rhaetian. **b** *Glomospira perplexa* FRANKE, 1936. Sample TGR138, Tiefengraben section, Upper Rhaetian. **c** *Trochammina squamosa* ZIEGLER, 1964. Tiefengraben section, TGR189, Uppermost Rhaetian. **d–e** *Trochammina canningensis* TAPPAN, 1955. Schlossgraben section, HC11, Uppermost Rhaetian. **f** *Pseudonodosaria multicostata* (BORNEMANN, 1854). Sample HC2, Schlossgraben section, Upper Rhaetian, fa- side view; fb- apertural view. **g** *Nodosaria claviformis* TERQUEM, 1866. Sample HC3, Schlossgraben section, Upper Rhaetian. **h** *Pseudonodosaria simpsonensis* (TAPPAN, 1951). Sample EB333, Eiberg section, Upper Rhaetian. **i** *Nodosaria nitidana* BRAND, 1937. Sample HC3, Schlossgraben section, Upper Rhaetian. **j** *Nodosaria anarthra* KRISTAN-TOLLMANN, 1964. Sample HC3, Schlossgraben section, Upper Rhaetian. **k** *Paralingulina tenera tenera* (BORNEMANN, 1854). Sample HC2, Schlossgraben section, Upper Rhaetian, ka- side view; kb- apertural view. **l** *Pseudonodosaria oculina* (TERQUEM & BERTHELIN, 1875). Sample HC3, Schlossgraben section, Upper Rhaetian, la- side view; lb- apertural view. **m** *Astacolus matutina* (D'ORBIGNY, 1850). Sample HC1, Schlossgraben section, Upper Rhaetian. **n** *Ichtyolaria bicostata* (D'ORBIGNY, 1849). Sample EB322, Eiberg section, Upper Rhaetian. **o** *Pseudonodosaria plurimicostata* (KRISTAN-TOLLMANN, 1964). Sample TGR97, Tiefengraben section, Upper Rhaetian. oa- side view; ob- apertural view. **p** *Ichtyolaria rhaetica* (KRISTAN-TOLLMANN, 1964). Sample EB322, Eiberg section, Upper Rhaetian. **q** *Lenticulina varians* (BORNEMANN, 1854). Sample HC2, Schlossgraben section, Upper Rhaetian. **r** *Astacolus filosa* (TERQUEM, 1866). Sample HC1, Schlossgraben section, Upper Rhaetian. **s** *Eoguttulina liassica* (STRICKLAND, 1846). Sample EB322, Eiberg section, Upper Rhaetian. **t–u** *Prodentalina paucicurvata* (FRANKE, 1936). Sample TGR52, Tiefengraben section, Upper Rhaetian. **v** *Astacolus pediacus* TAPPAN, 1955. Sample TGR193, Tiefengraben section, Upper Rhaetian. **w** *Lenticulina gottingensis* (BORNEMANN, 1854). Sample HC1, Schlossgraben section, Upper Rhaetian. **x** *Ammomarginulina beggi* STRONG, 1984. Sample EB385, Eiberg section, Upper Rhaetian. xa- side view; xb- apertural view. **y** *Ammobaculites* cf. *duncani* SCHROEDER, 1968. Sample TGR131, Tiefengraben section, Upper Rhaetian. **z** *Pseudonodosaria limpida* (WOSZCZYNSKA, 1987). Sample TGR97, Tiefengraben section, Upper Rhaetian. za- side view; zb- apertural view

In the deeper part of the Eiberg basin (Eiberg and Schlossgraben sections), the influence of the end-Triassic sea level drop on the foraminiferal assemblages is not marked. In the uppermost Eiberg Mb (transition to the Tiefengraben Mb) the persistence of abundant and diversified Nodosariidae within the marly interval still records outer shelf conditions with normal marine salinity conditions, as also attested to by the $\delta^{18}O$ and $\delta^{13}C_{carb}$ values (Fig. 6). Nonetheless, in this stratigraphic interval first symptoms for a change in the marine environment do occur (Fig. 6). Assemblages consisting of infaunal fine-agglutinated taxa (*Ammobaculites* cf. *duncani, Ammomarginulina beggi*; Fig. 6c) mark the shift from deposit to detritus feeders and bacterial scavengers, tolerant to low-oxygen and organic matter of continental origin (Nagy 1992; Tyszka 1994; Kuhnt et al. 1996; Kaminski et al. 1999; Alegret et al. 2003; Reolid et al. 2008). Their presence is related to the pattern of high $\delta^{18}O$ and type III OM values indicating a possible continental origin (see Sect. "Characterisation of organic matter"), and high $\delta^{18}O$ (Fig. 6). High $\delta^{18}O$ values can be interpreted in terms of cooling or salinity increase. We excluded salinity increase, because it is incompatible with ecological preferences of agglutinated foraminifera. They generally prefer low pH conditions and/or cold waters and/or brackish conditions. We excluded also brackish conditions, because in this case both decreasing of $\delta^{13}C_{carb}$ and $\delta^{18}O$ values are expected. Therefore, the combination of foraminifera and geochemistry points to a cooling event and/or seawater chemistry change (lower pH). The marked peak in the abundance of the aragonitic Involutinidae *Trocholina* (Fig. 6) in the topmost part of Eiberg section could be related to a relative

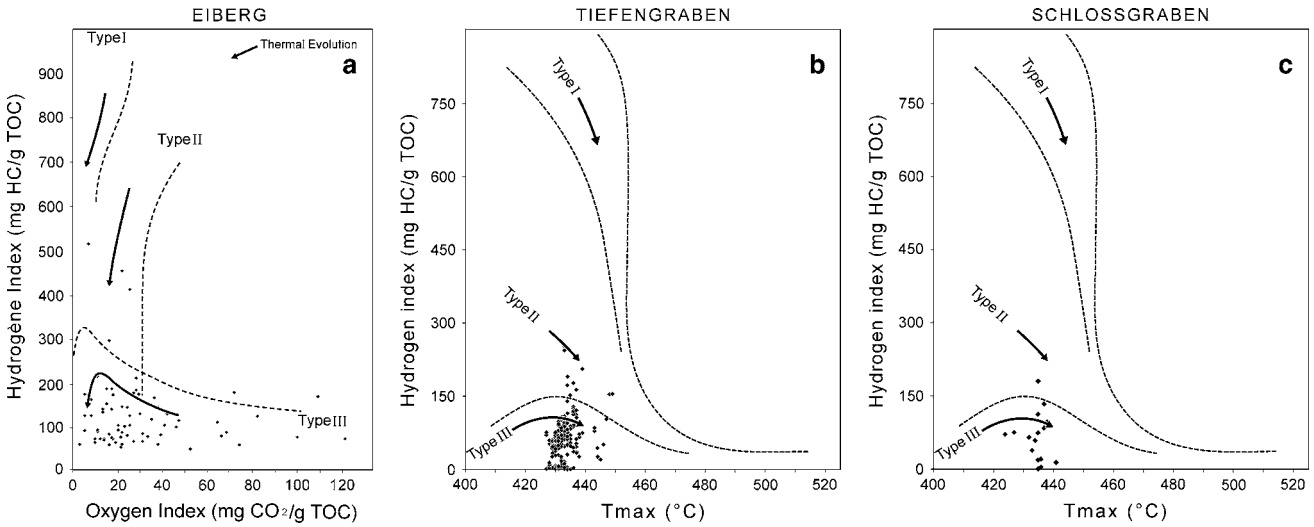

Fig. 13 **a** Eiberg TOC results plotted in a modified Van Krevelen diagram (HI vs. OI). **b–c** Tiefengraben and Schlossgraben TOC data plotted in a HI vs. T_{max} diagram (Espitalié et al. 1985a, b, c), respectively. The three sections display a continental/oxidated OM contribution of Type III except for three samples from the Eiberg section (from the base of the thick calcareous interval), characterized by preserved marine OM of Type II

Table 1 Calcareous nannofossil and benthic foraminifera assemblages of the Eiberg and Schlossberg sections

Section	Assemblage		Occurrence in section (m)	Characteristic	Other
Schloss	Sch + Co	Nanno	From 0.5 to 0.11	Schizosphaerellids (40%) *Conusphaera* spp. (35%)	*Obliquipithonella spp.* (<10%)
Schloss	Pt3	Nanno	From base to 0.5	*P. triassica* (40%) with small forms *Conusphaera* spp. (25%)	*P. triassica*, (<20%), *Obliquipithonella* spp. (<10%)
Schloss	TROCHA	Benthic forams	From 0.11 to 0.20	Very abundant (~6,500 ind./g of sed.) and low diversified agglutinated taxa. *Trochammina canningensis*	
Schloss	DN	Benthic forams	From base to 0.11	Abundant (~2,500 ind./g of sed.), diversified hyaline Nodosariidae *Lenticulina varians, L. subquadrata Astacolus.* aff. *A. dorbignyi*, *A. semi-incisa, A. matutina Ichthyolaria rhaetica P. tenera Nodosaria anarthra*, *N.claviformis*, *N. nitidana Pseudonodosaria multicostata*	
EIBERG	CC + Sch	Nanno	From 20 to the top	*Obliquipithonella* spp. + *Orthopithonella* spp. (30–50%)	Schizosphaerellids (10%)
				E. zlambachensis + *E. tollmanniae* (25–30%)	
EIBERG	Pt3	Nanno	From 19 to 20	*P. triassica* (40%) with small forms *E. zlambachensis* + *E. tollmanniae* (~30%)	*Obliquipithonella* spp. (20%)
					Orthopithonella spp. (10%)
					Coccoliths (<1%)
EIBERG	Pt2	Nanno	From 16.6 to 19	*P. triassica* (50–80%) with medium and small forms *E. zlambachensis* + *E. tollmanniae* (~20%)	*Obliquipithonella* spp. (10–20%)
					Orthopithonella spp. (<5%)
					Coccoliths (<1%)
EIBERG	Pt1	Nanno	From 4 to 7.5 and 16.5	*P. triassica* (50–80%) with large forms *E. zlambachensis* + *E. tollmanniae* (40%)	*Orthopithonella* spp. (15%)
					Obliquipithonella spp. (<5%)
					Coccoliths (<1%)
EIBERG	TROCHO	Benthic forams	From 19 to 20	Very abundant aragonitic involutinidae (~15,000 ind./g of sed.) *Trocholina* cf. *T. verrucosa*	Abundant (~4,000 ind./g of sed.) and diversified hyaline: Nodosariidae (*L. gottingensis*, *P. simpsonensis*, *P. turgida*), *E. liassica* (~1,600 ind./g of sed.), *Glomospira perplexa* (~250 ind./g of sed.)
EIBERG	AG	Benthic forams	From 16 to 17.5	Low abundance (~200–900 ind./gram of sed.) and low diversified fine agglutinated taxa. *Ammobaculites rhaeticus Ammomarginulina beggi*	Very rare hyaline taxa (<20 ind./g of sed.)
EIBERG	DN	Benthic forams	From 16.5 to the top and, from 4 to 8	Abundant (~5,000 ind./g of sed.), diversified hyaline Nodosariidae. *Lenticulina gottingensis*	Polymorphinidae (~800–1,600 ind./g of sed.), *Eoguttulina liassica*
				Pseudonosaria simpsonensis	
				Prodentalina turgida	
				Ichtyolaria bicostata, I. rhaetica	

Calcareous nannofossil assemblages: Pt1, *P. triassica* assemblage with large forms; Pt2, *P. triassica* assemblage with small to medium-sized forms; Pt3, *P. triassica* assemblage with small forms; CC + Sch, calcareous cysts + "Schizosphaerellids" assemblage; Sch + Co, "Schizosphaerellids" + Conusphaerids. Benthic foraminifera assemblages: DN, diversified nodosariidae; AM, *Ammobaculites-Ammomarginulina*; TROCHO, *Trocholina;* TROCHA, *Trochammina*

Table 2 Calcareous nannofossil and benthic foraminifera assemblages of the Tiefengraben section

Section	Assemblage		Occurrence in section (m)	Characteristic	Other
Tiefengraben	PA + Sch	Nanno	From 17 to the top	Sparse small *P. triassica* and Schizosphaerellid fragments	
Tiefengraben	PA	Nanno	From 12 to 15	Sparse *P. triassica*	
Tiefengraben	Pt1	Nanno	From 0 to 1.5	*P. triassica* (20%) *E. zlambachensis* + *E.tollmanniae* (10-15%)	*Orthopithonella* spp. (<10%) *Obliquipithonella* spp. (<10%) Coccoliths (<1%)
Tiefengraben	PA	Benthic forams	From 23 to the top	Low abundant (~200 ind./g of sed.) and low diversified hyaline Nodosariidae. *Paralingulina tenera*	Very rare (<10 ind./gram of sed.) agglutinated taxa
Tiefengraben	AM	Benthic forams	From 17 to 23	Low abundant (<1,000 ind./g of sed.) and low diversified coarse agglutinated taxa. *Ammobaculites* cf. *duncani, Ammomarginulina beggi*	Low abundant (~100–300 ind./g of sed.) of small size hyaline taxa. *Pseudonodosaria limpida*
Tiefengraben	TROCHA	Benthic forams	From 13 to 15	Very abundant (~5,000 ind./g of sed.) low diversified agglutinated taxa. *Trochammina squamosa, Glomospira perplexa*	Very rare (<40 ind./g of sed.) hyaline taxa
Tiefengraben	DN	Benthic forams	From 0 to 1.5	Abundant (~1,000 ind./g of sed.), diversified hyaline Nodosariidae. *Pseudonodosaria limpida, P. plurimicostata, Prodentalina subsiliqua, P. paucicurvata, Astacolus pediacus*	Low abundant Polymorphinidae (~200 ind./g of sed.). *Eoguttulina liassica*

Calcareous nannofossil assemblages: Pt1, *P. triassica* assemblage with large forms; PA, poor assemblage; PA + Sch, poor assemblage + "Schizosphaerellids". Benthic foraminifera assemblages: DN, diversified Nodosariidae; TROCHA, *Trochammina*; AM, *Ammobaculites-Ammomarginulina*; PARA, *Paralingulina tenera*

sea-level drop (transition from outer to mid shelf environments, around 50 m water depth), although fully marine conditions are still maintained, as shown by the presence of abundant Nodosaridae and by $\delta^{13}C_{carb}$ and $\delta^{18}O$ values. In Mesozoic sediments, *Trocholina*, interpreted as primary seaweed fauna, is often associated with shallow-water facies (Reolid et al. 2008).

In fully marine conditions and with a limited diagenetical impact compared with Tiefengraben and Kendelbach sections, the Schlossgraben section records a peak of agglutinated *Trochammina* (Fig. 7c) across the Kössen and the Kendelbach Formation transition, in coincidence with the end Triassic $\delta^{13}C_{org}$ negative excursion. Genus *Trochammina* has been variously interpreted as an epifaunal, detritivore/scavenger feeder and omnivore active consumer of bacteria or herbivore (Jones and Charnock 1985; Nagy 1992). In modern environments, *Trochammina* has been found to survive in marshes with extreme chemical pollution and low pH (for example in the S. Francisco Bay, McGann and Sloan 1999). A similar *Trochammina* assemblage has been found in the most marginal setting of the Eiberg basin, such as Tiefengraben and Kendelbach, where the sea-level drop in the latest Triassic has been much more significant (Golebiowski 1990; Kuerschner et al. 2007). At Tiefengraben, Kendelbach and Schlossgraben the absence of hyaline foraminifera and the occurrence of *Trochammina* (perhaps enhanced by selective dissolution, as mentioned previously) at the end-Triassic may indicate stressful conditions (Figs. 7c, 8, 9b). These are probably related to temporary pH reduction. However, at Tiefengraben and Kendelbach this lowering of pH is likely due in part to brackish conditions, as indicated by low values of both $\delta^{13}C_{carb}$ and $\delta^{18}O$ (Marshall 1992) and other palaeontological proxies such as palynomorphes and bivalves (Golebiowski 1990; Kuerschner et al. 2007).

At Tiefengraben, the composition of the agglutinated foraminiferal assemblage undergoes changes at the early Hettangian $\delta^{13}C_{org}$ negative excursion. Here, the assemblage is characterized by a low abundance of the infaunal detritivores *A.* cf. *duncani* and *A. beggi,* often associated with small hyaline infaunal *P. limpida* (Fig. 9b). This assemblage mirrors persisting shallow-water brackish environments, probably characterized by low oxygen conditions. In particular, coarsely-agglutinated *Ammobaculites* from Jurassic sediments have been previously interpreted as shallow-water forms associated with reduced salinity or oxygenated environments (Jenkins and Murray 1989; Hemleben et al. 1990). Further upward, at the transition to the Breitenberg Mb, renewed dominance of Nodosariidae with *Paralingulina tenera* (Fig. 9b) may reflect a sea-level rise and the re-establishment of more open-marine conditions (Jenkins and Murray 1989). This is associated with a peak of marine palynomorphs (Kuerschner et al. 2007), and the occurrence of a more open, normal-marine fauna with brachiopods, bivalves and ammonoids (Golebiowski 1990).

Palaeoecology of late Triassic calcareous nannofossils

The biological affinities, ecological preferences and stratigraphic succession of Late Triassic calcareous nannofossils are not known. They represent a complex group, whose specimens are difficult to compare to modern phytoplankton taxa (Eventually you could provide a reference). Therefore, interpretations concerning the ecological preferences of *Prinsiosphaera triassica*, Conusphaerids (*Eoconusphaera zamblachensis* and *Eoconusphaera tollmaniae)*, Schizosphaerellids, and of calcareous cysts (*Orthopithonella* and *Obliquipithonella*) remain tentative at best.

In the uppermost Eiberg section, the reduction in size of *P. triassica* and its decrease in abundance broadly occur together with major positive $\delta^{18}O$ shifts which might be interpreted as cooling pulses, sea-water chemical changes and/or decreasing pH, as also inferred for benthic foraminifers (see previous paragraph). These data might suggest that the abundance of *P. triassica* was preferentially favoured by warm seawaters, probably with high availability of HCO_3^- content. *P. triassica* is very abundant in Rhaetian limestones (Gardin, personal observation) and it was probably an important contributor to the formation of carbonate sediments at that time. Its thick wall structure could also indicate a benthic life-stage in epicontinental shelf environments, as inferred for some calcareous dinoflagellates (Kohring et al. 2005). However, although *P. triassica* resembles calcareous dinoflagellates in size and shape, it possesses a solid structure and lacks a consistent archaeopyle when compared with calcareous dinoflagellates.

Conusphaerids are very abundant in the upper Rhaetian (Fig. 5b, 7b, 8b), and they are also reported to be very abundant and "rock-forming" in Late Jurassic sediments, possibly indicating a deep nutricline and oligotrophic/cooler surface water conditions (Bornemann et al. 2003). In this study, the general trend in the relative abundance of Conusphaerids is inversely correlated to the relative abundance curve of *P. triassica* (Fig. 5b), indicating that these nannoliths inhabited different ecological niches and/or responded to divergent environmental parameters.

With the broad term "Schizosphaerellid" we group calcareous nannofossils presenting shape and optical properties almost identical to the Jurassic genus *Schizosphaerella* when observed under the optical microscope (Fig. 11d–f). *Schizosphaerella* prevails in carbonate-rich sediments and is interpreted as a nannolith that preferentially inhabited proximal environments (Noël et al. 1994; Mattioli 1997; Cobianchi and Picotti 2001; Mattioli and

Pittet 2004). Two hypotheses have been proposed to explain the palaeoecological preferences of *Schizosphaerella*: (1) an oligotrophic, deep-dwelling habitat (Claps et al. 1995; Erba 2004; Tremolada et al. 2005) or (2) a mesotrophic shallow-dwelling habitat (Mattioli and Pittet 2004). Our results on Triassic "Schizosphaerellids" show a clear increase in abundance during the uppermost Rhaetian, just before the first negative CIE (Eiberg and Schlossgraben sections) but cannot support any of the two proposed palaeocological hypotheses.

Calcareous cysts (*Orthopithonella* spp. and *Obliquipithonella* spp.) are known since the Late Triassic in both the Mediterranean and Boreal realms (Villain 1981; Janofske 1987) but their affiliation to calcareous-walled dinoflagellates was recently questioned (Gottschling et al. (2008). Modern calcareous dinoflagellate cysts are present from neritic to pelagic marine environments (Wall and Dale 1968; Dale 1983, 1986). Their ecological preferences are species-specific, but important information can be gathered from cyst size and wall structure, which are often influenced by water mass parameters (Keupp 1995, 2001; Keupp and Mutterlose 1994). Large cysts seem to occur in warmer waters, whereas smaller ones correspond to cooler water masses (Kohring et al. 2005). Sea-level changes may also control the phenotypical variability and palaeogeographical distribution of calcidinocysts (Keupp 1995; Keupp and Kowalski 1992; Zügel 1994). In our study, abundant calcareous cysts were observed in the Kössen Formation. Reduction in size and increasing abundance are observed in the uppermost Eiberg section synchronously with $\delta^{13}C_{carb}$ decreasing and $\delta^{18}O$ increasing trends, while a clear decrease in abundance is observed from the very top of the T-Bed in Schlossgraben (Figs. 4b, 5b, 8b). Although it is hard to outline unequivocal ecological preferences for Rhaetian calcareous cysts from the present study, their biotic pattern in the Eiberg basin concurs with with lowered surface productivity and establishment of cooler surface waters.

The ecological preferences of the Triassic coccoliths *Crucirhabdus minutus*, *C. primulus* and *Arkeozygodiscus koessenensis* are not inferred due to their low abundance. In this study, they are not observed above the Tr-J boundary.

Discussion

Calcareous nannoplankton are tracers of both organic and inorganic carbon pumping with an obvious major impact on atmosphere/ocean interactions (Rost and Riebesell 2004). Thus, in response to environmental changes, the primary surface productivity plays a major role in the vertical flux of organic carbon with ballast minerals sinking into the deep sea (Barker et al. 2003). Thanks to their great sensitivity to nutrient supply exported from the surface (main source of food), benthic foraminifera can record direct positive or negative feedbacks in response to modifications of the primary productivity. In fully marine conditions, if a bentho-planktonic linkage is observed, it can mimic the functioning of biological pumping (primary productivity and export production). In this study, the qualitative and quantitative modifications observed in calcareous nannofossil assemblages seem faithfully recorded at the bottom by qualitative and quantitative changes in benthic foraminifera assemblages. However, the latter are also influenced by the continental organic matter input, which increased during the ongoing end-Triassic sea-level fall. At Tiefengraben, the influence of the sea-level fall on the calcareous nannofossil and foraminifera assemblages is even more prominent. The combination of micropaleontological and geochemical data, allows us to propose a multi-phase environmental disruption across the end-Triassic carbon isotope negative excursion (Fig. 14).

Pre-perturbation interval

In the Late Rhaetian (Eiberg and Tiefengraben sections), calcareous nannofossil assemblages fluctuate highly in phase with large-sized epifaunal-infaunal, calcareous benthic foraminifera (Figs. 4, 5, 6, 7, 8, 9) and with TOC, $CaCO_3$ and $\delta^{13}C_{carb}$ values. These "pre-perturbation" bentho-planktonic linkages might indicate a well-structured trophic chain and good recycling of nutrients (as also attested by type II organic matter), in an oxygenated and mixed water column. The abundant and diversified calcareous benthic foraminifera translate as a flux of good labile marine organic matter (phytodetritus).

Onset of perturbation

P. triassica fluctuates in abundance and size all along the studied sections, but a decline is observed in the uppermost Rhaetian at Eiberg (from 16 to 20 m; Figs. 4b, 5b). Since the "thick" structure of *P. triassica*'s had more potential in producing $CaCO_3$ than the "hollow" structure of calcareous cysts, the reduction in size and abundance of the former and the increase of the latter, probably affected the surface carbonate production and vertical export to the sea-bottom. This disturbance seems to be reflected by the decreasing trend of the isotope carbon curve as well as reduced abundance and change in composition of the benthic foraminifers (Fig. 6b, c). The latter may record a decreasing flux of marine organic matter at the sea-bottom, and/or an increasing supply of continental OM related to the latest Triassic regression. We interpret this biotic pattern as the onset of a decline in surface carbonate production in the Eiberg Basin, starting from the major positive shift of the

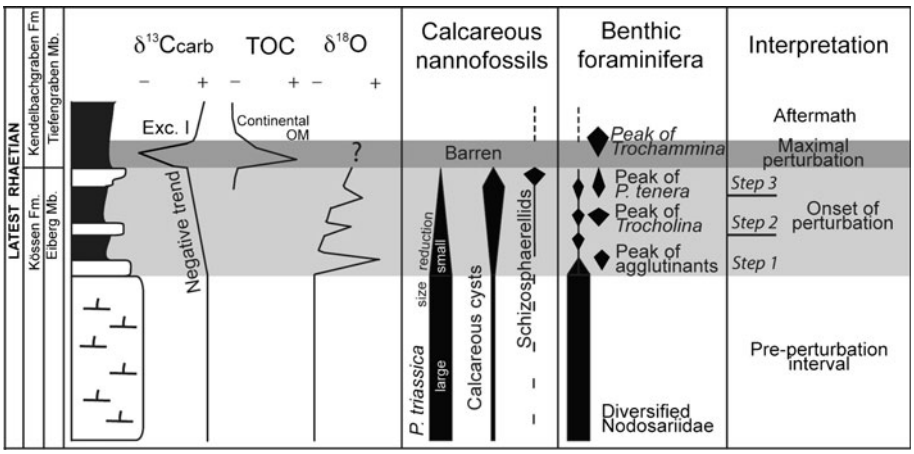

Fig. 14 Biotic patterns of calcareous nannofossils and benthic foraminifera across the end-Triassic crisis

$\delta^{18}O$ curve (heaviest values) and taking place in three progressive steps, each linked to $\delta^{18}O$ fluctuations and to the presence of probable continental OM due to a falling sea-level. The major positive shift of the $\delta^{18}O$ curve represents a major palaeoenvironmental deterioration, probably related to a short-term cooling "pulse" and/or seawater chemistry/pH change responsible for the demise of large *P. triassica* and overall smaller size of calcareous nannofossils (Fig. 4b). It is accompanied by changes in feeding strategies at the sea-floor, first (step 1 in Fig. 14) with the development of shallow, fine detritivore, agglutinated foraminifera (*Ammobaculites-Ammomarginulina*; Fig. 4b). Later on (step 2, Fig. 14), calcareous nannofossil assemblages are characterized by overall small-size specimens (Fig. 4b) while the foraminifera assemblage is dominated by low abundant infaunal, hyaline foraminifera (*Pseudonodosaria simpsonensis*), possibly indicating transient dysaerobic conditions (Fig. 6b). Finally (step 3, Fig. 14), *P. triassica* reaches its lowest abundance, while calcareous cysts also decrease and Schizosphaerellids increase (Fig. 5b). Thus, perturbation in nannofossil productivity, expressed by reduction in size and changes in the proportions of the carbonate primary producers, are transferred to the sea-floor: benthic foraminifera seem to explicitly record the reduction of marine organic matter flux, as a consequence of decreased ballast effect (Barker et al. 2003).

The three steps of perturbation of the surface carbonate production alternate with conditions during which *P. triassica* and hyaline foraminifera get back to higher abundance, suggesting a better efficiency of the export pathway within the water column down to the sea floor (Figs. 5b, 6b, 7). However, the huge increase in active herbivores-phytodetritivores epifauna (*Trocholina* cf. *T. verrucosa*; Fig. 6b), shortly before the third step could be related to a falling sea-level and a major continental influence (see Sect. "Characterisation of organic matter"), rather than to the export production within the water column. The development of "Schizosphaerellids", starting at the very end of the Rhaetian (Figs. 5b, 7b), is rapidly interrupted at the same time as a major negative excursion of $\delta^{13}C_{carb}$ and $\delta^{13}C_{org}$ at the end-Triassic is observed. It is interesting to note that this development coincides with a slight increase (1%) of organic matter and of infaunal benthic foraminifera (*Nodosaria* spp. + *Paralingulina tenera*), which might represent a temporal increase of phytodetritus and/or reduction of oxygen level at the sea-bottom (Fig. 7; Jorissen et al. 1995; Mailliot et al. 2009).

Maximal perturbation

In the latest Triassic, in both the Schlossgraben and Tiefengraben sections, assemblages severely deprived of micro- and nannofossils represent a maximal environmental deterioration process, associated with the first negative $\delta^{13}C_{carb}$ $\delta^{13}C_{org}$ shift and an abrupt decrease of the $CaCO_3$ content (Figs. 7, 8). The sea-level lowstand played a significant role probably inducing important salinity variations, as suggested by Kuerschner et al. (2007). The reduced salinity of surface waters possibly led to a salinity-stratification of the water column and might have reduced the oxygen level at the bottom of the Eiberg basin, promoting the preservation of organic matter (Bonis et al. 2009). The organic-rich level at Schlossgraben is probably of continental origin (type III, see Sect. "Characterisation of organic matter") and related to the regression and decreasing carbonate sedimentation. However, in other sections of the Eiberg basin, marine organic matter enrichment has been documented in coincidence with the first CIE (Ruhl et al. 2009). Yet, the abruptness of the Austrian negative $\delta^{13}C$ shift (Kuerschner et al. 2007; Ruhl et al. 2009) suggests a discontinuity surface (hiatus) on top of Kössen Formation, linked to the end-Triassic maximal sea-level fall. At Tiefengraben and Schlossgraben, there is no sedimentological evidence of emersion.

Therefore, we interpreted this hiatus as an extreme reduction of carbonate sedimentation (Hautmann 2008).

Aftermath

Synchronously with the onset of $\delta^{13}C_{org}$ recovery, at Tiefengraben, Kendelbach and at Schlossgraben, calcareous nannofossil assemblages are barren while benthic foraminifera consist almost exclusively of *Trochammina*, which occur in high abundances (Figs. 7c, 8, 9b). The latter could be interpreted as a "disaster scavenger feeder" typical of devastated marine ecosystems, within a unstable environment. The strong environmental tolerance of *Trochammina,* regardless of extreme environmental conditions (chemical pollution, pH), may attest to seawater acidification.

The interpretation of the biotic pattern could be biased by local facies and palaeoenvironmental changes. In fact, at the end-Triassic and continuing into the earliest Hettangian, the Tiefengraben section is under strong continental influence, as clearly suggested by organic matter and palynological observations (Kuerschner et al. 2007; Ruhl et al. 2009). Therefore, the local influence of the shallow-brackish environment at Tiefengraben probably enhanced the marine environmental deterioration that started in the Late Triassic, and lead to a maximal perturbation. However, we emphasize that in the Schlossgraben section, under more marine influence (Hillebrandt and Krystyn (2009), similar assemblages are present (Fig. 7), probably indicating a more general biotic signal.

Global scenario of carbonate production and the end-Triassic crisis

The latest Rhaetian pre-CIE positive $\delta^{18}O$ peaks observed in Austria, are symptomatic of a marine environmental deterioration starting with a decrease in surface carbonate production and culminating in a complete cessation of the pelagic carbonate production.

The demise and extinction of the most abundant component of calcareous nannofossils assemblages, *P. triassica,* represents a significant event leading to a dramatic change in surface carbonate producers across the Triassic-Jurassic boundary. *P. triassica* was dominant during the late Rhaetian, suffered a reduction in abundance and size and finally it was replaced by calcareous cysts and by "Schizosphaerellids" before its final extinction. The end-Triassic crisis was severe for calcareous nannofossils. However, some nannoliths (Conusphaerids) as well as calcareous cysts (*Orthopithonella*, *Obliquipithonella)* and coccolith *Crucirhabdus* reappeared with new species during the Jurassic.

The reasons for the disappearance of the "*Prinsiosphaera* world" at the end-Triassic remain unknown, but cooling and sea-level fall might have severely affected its ecological niche. Recent reconstructions suggest a link between nannoplankton evolution and sea-level changes, with high extinction rates and major turnovers often coinciding with regressions (Erba 2006). Alternatively, *Prinsiosphaera*'s extinction might be linked to changes in sea-water chemistry. Its thick structure could have been favoured by a $CaCO_3$ hyper-saturation state of shallow seawaters on the continental shelf, primary locus of the carbonate deposition at that time ("Neritan" ocean mode; Zeebe and Westbroek 2003; Ridgwell 2005). A "Late Triassic supercalcification" is supported by other fossil evidence as the spectacular accumulation of reef limestones along the southern Tethyan margin (Martini et al. 2000). We speculate that the crisis of "supercalcifiers" (e.g., reef building scleractinian corals) as well as the definitive demise of *P. triassica* at the very end of the Triassic was likely due to a major change in surface $CaCO_3$ Ω and pH, coupled with a global regressive trend. Perhaps *P. triassica,* contrary to other calcareous nannofossils, had a minor physiological control on biocalcification and was more vulnerable to changes in seawater chemistry (Stanley 2006).

A large-scale, end-Triassic carbonate crisis is reported from sections of different palaeogeographical domains (Stanley 2003; Hesselbo et al. 2002; Guex et al. 2004; Hautmann 2004, 2008; Galli et al. 2005). The shut-down of the "carbonate factory" resulted in a widespread hiatus or extreme condensation in coincidence with the end-Triassic carbon negative shift (Hautmann 2004). Carbonate crises are characteristic of major extinction intervals linked with the occurrence of large igneous provinces (Courtillot and Renne 2003), and the temporal coincidence of CAMP volcanism with the end-Triassic crisis is now well-documented (Marzoli et al. 2004; Schaltegger et al. 2008; Cirilli et al. 2009; Schoene et al. 2010). Some authors relate the rise in the flux of volcanogenic CO_2 to the atmosphere, and possibly methane release from gas-hydrate dissociation, which led to temporary acidification of the surface ocean and under-saturation of seawater with respect to aragonite and calcite (Hautmann 2004, 2008; Galli et al. 2005). Leaf stomatal indices have been taken as evidence of such induced CAMP "lethal" super greenhouse warming across the Tr-J boundary (McElwain et al. 1999). On the other hand, the highly discontinuous and incomplete continental record reduces the temporal resolution of this palaeobotanical proxy and the correlation with marine record is unclear. Moreover, leaf stomatal features might have not a straightforward, linear relationship with atmospheric CO_2 and they could be related to other environmental stress factors, such as volcanogenic SO_2 (Tanner et al. 2007).

Repeated releases of SO_2 by CAMP volcanism (Tanner et al. 2001; McHone 2002; Guex et al. 2004; van de Schootbrugge et al. 2009) coupled with the major regression observed at the end-Triassic stage could have triggered the marine environmental perturbation. The impact of volcanism on climate and palaeoenvironmental conditions is linked to several factors (lava composition, eruption rate, etc.) among which the amount and composition of volatile gases (mainly CO_2 and SO_2), and the altitude reached by the volcanic plume (Textor et al. 2004). It is now apparent that sulphur plays the leading role in cooling climatic events (Chenet et al. 2005; Self et al. 2006). Sulphur-rich gases (1–25%) released into the stratosphere are rapidly converted to sulphate aerosols, which result in reduced insolation and cooling of the lower troposphere. Besides the climatic impact, the reduced insolation has direct adverse impacts on both photosynthesis and primary productivity. Sulfuric emissions, together with other pollutants (Guex et al. 2004; Chenet et al. 2005), are concentrated in the stratosphere, forming acidic fog near the Earth's surface. It could have generated dramatic modifications of the carbonate seawater chemistry through acidification, affecting CO_2 exchange between atmosphere and ocean, and the primary carbonate production. Model results assessing the impact of CAMP volcanism on ocean carbonate chemistry done by Berner (2007) suggest that volcanic SO_2 could have significantly promoted dissolution and ocean undersaturation with respect to calcite. The observed decreased in abundance and in size of some calcareous nannofossils could hence be explained by ocean acidification and cooling caused by major CAMP volcanic eruption pulses. The "cooling" hypothesis is also consistent with the interpretation of Hubbard and Boulter (2000), who proposed a dramatic and protracted "cold event" during the latest Triassic, on the basis of palynological data.

Changes in the ecological success of calcifying organisms caused by ocean acidification might have affected the biological carbon pump, for example through the inhibition of calcification processes. In the same way, the average change of "calcispheres" diameter might indicate undercalcified specimens linked to the cooling episode, and maybe also to low pH conditions. Consequently, the carbonate balance of the oceans might have been affected, favouring the increase of carbonate solubility. This way, the ecological balance could have shifted in favour of non-calcifying organisms, such as organic-walled phytoplankton (van de Schootbrugge et al. 2007; Götz et al. 2009; Bonis et al. 2009), and agglutinated foraminifera specimens (this study). All these factors may have had a "knock-out" effect on the sinking of organic material (export production) and biological pump functioning, as expressed by the observed bentho-planktonic relationship.

Conclusions

This paper presents a first synecological study of calcareous nannofossils and benthic foraminifera from three austrian sections which argues strongly of a marine ecosystem deterioration starting during the late Rhaetian and culminating in carbonate pump collapse at the end of Triassic.

During the late Rhaetian, surface carbonate production dropped due to : (1) a decrease in abundance and size of calcareous nannofossil *P. triassica* and its final extinction at the end-Triassic; (2) increase of calcareous cysts and "Schizosphaerellids", with a lesser potential of carbonate production. These surface-water modifications are expressed at the sea-bottom by the development of detritus-feeding agglutinated foraminifera (*Ammobaculites, Ammomarginulina*). The clear link between planktonic and benthic assemblages further points to a disturbance of the biological carbonate pump.

The paroxysmal phase of the end-Triassic crisis is revealed by assemblages devoid of calcareous micro- and nannofossils, in association with a $\delta^{13}C$ negative shift. This biological collapse is immediately followed by the development of *Trochammina* "disaster scavenger feeder" benthic foraminifera.

The end-Triassic biotic crisis might have been generated by the onset of the CAMP paroxysmal activity, which in turn imposed a major worldwide regressive phase. Volcanogenic SO_2 emissions might be responsible of the establishment of the major cooling episode, seawater chemistry changes and/or low pH conditions at the end of the Triassic stage.

Acknowledgments We thank François Baudin, Helmut Weissert, Rossana Martini and Emanuela Mattioli for fruitful discussions, Leopold Krystyn and Axel von Hillebrandt for precious field-trip information and Sally Reynolds and Alain Morard for English text assistance. The manuscript has benefited from the constructive reviews of E. Erba and L. Tanner, for which they are gratefully thanked. We also thank Joel Ughetto (MNHN UMR 7209) for isotope data and Gérard Mascarell (FRE 3206 CNRS/MNHN) for MEB photo assistance. This research was supported by the CNRS Program Project "Eclipse II", and by IFP, Convention no 31231, by the Swiss NSF project 200020-111559 and by the MNHN PPF "Biodiversité et role des microorganismes dans les écosystèmes actuels et passés". We acknowledge the Région Ile de France, which contributed toward the purchasing of the mass spectrometer of SSMIM (Muséum National d'Histoire Naturelle of Paris, France).

References

Alegret, L., Molina, E., & Thomas, E. (2003). Benthic foraminiferal turnover across the cretaceous/paleogene boundary at Agost (southeastern Spain): Palaeoenvironmental inferences. *Marine Micropaleontology, 48*, 251–279.

Barker, S., Higgins, J. A., & Elderfield, H. (2003). The future of the carbon cycle: Review, calcification response, ballast and feedback on atmospheric CO_2. *Philosophical Transactions: Mathematical, Physical and Engineering Sciences, 361*(1810), 1977–1999.

Behar, F., Beaumont, V., & Penteado, H. L. De B. (2001). Rock-eval 6 technology: Performances and Developments. *Oil & Gas Science and Technology—Revue IFP*, *56*(2), 111–134.

Bellanca, A., Di Stefano, P., & Neri, R. (1995). Sedimentology and isotope geochemistry of Carnian deep-water marl/limestone deposit from the Sicani mountains, Sicily: Environmental implications and evidence for a planktonic source of lime mud. *Palaeogeography, Palaeoclimatology, Palaeoecology, 114*, 111–129.

Berner, R. A. (2007). Volcanic degassing necessary to produce a $CaCO_3$ undersaturated ocean at the Triassic-Jurassic boundary. *Palaeogeography, Palaeoclimatology, Palaeoecology, 244*, 368–373.

Bonis, N. R., Ruhl, M., & Kürschner, W. M. (2009). Climate change driven black shale deposition during the end-Triassic in the western Tethys. *Palaeogeography, Palaeoclimatology, Palaeoecology, 290*(1–4), 151–159.

Bornemann, A., Aschwer, U., & Mutterlose, J. (2003). The impact of calcareous nannofossils on the pelagic carbonate accumulation across the Jurassic-Cretaceous boundary. *Palaeogeography, Palaeoclimatology, Palaeoecology, 199*, 187–228.

Bown, P. R. (1987). Taxonomy, biostratigraphy, and evolution of late Triassic-early Jurassic calcareous nannofossils. *Special Papers in Palaeontology, 38*, 1–118.

Bown, P. R., & Young, J. R. (1998). Techniques. In P. R. Bown (Ed.), *Calcareous nannofossil biostratigraphy* (pp. 16–28). London: British Micropalaeontological Society Series, Chapman and Hall/Kluwer Academic Press.

Bralower, T. J., Bown, P. R., & Siesser, W. G. (1991). Significant of upper Triassic nannofossils from the southern hemisphere (ODP Leg 122, Wombat Plateau, N.W. Australia). *Marine Micropaleontology, 17*, 119–154.

Chenet, A. L., Fluteau, F., & Courtillot, V. (2005). Modelling massive sulphate aerosol pollution, following the large 1783 Laki basaltic eruption. *Earth and Planetary Science Letters, 236*, 721–731.

Cirilli, S., Marzoli, A., Tanner, L., Bertrand, H., Buratti, N., Jourdan, F., et al. (2009). Latest Triassic onset of the central atlantic magmatic province (CAMP) volcanism in the fundy basin (Nova Scotia): New stratigraphic constraints. *Earth and Planetary Science Letters, 286*, 514–525.

Claps, M., Erba, E., Masetti, D., & Melchiorri, F. (1995). Milankovitch-type cycles recorded in Toarcian black shales from the Belluno trough (Southern Alps Italy). *Memorie di Scienze Geologiche, 47*, 179–188.

Clémence, M. E., Bartolini, A., Gardin, S., Paris, G., Beaumont, V., Page, K. (2010). Early Hettangian benthic-planktonic coupling at Doniford (SW England). Palaeoenvironmental implications for the aftermath of the end-Triassic crisis. *Palaeogeography, Palaeoclimatology, Palaeoecology*. doi:10.1016/j.palaeo.2010.05.021

Cobianchi, M., & Picotti, V. (2001). Sedimentary and biological response to sea-level and palaeoceanographic changes of a lower–middle Jurassic Tethyan platform margin (Southern Alps, Italy). *Palaeogeography, Palaeoclimatology, Palaeoecology, 169*, 219–244.

Courtillot, V., & Renne, P. R. (2003). On the ages of flood basalt events. *Comptes Rendus Geoscience, 335*, 113–140.

Dale, B. (1983). Dinoflagellate resting cysts, "benthic plankton". In G. A. Fryxell (Ed.), *Survival strategies of the algae* (pp. 69–136). Cambridge: Cambridge University Press.

Dale, D. (1986). Life cycle strategies in oceanic dinoflagellates. *UNESCO Technical Paper: Marine Sciences, 49*, 65–72.

Di Nocera, S., & Scandone, P. (1977). Triassic nannoplankton limestones of deep basin origin in the central Mediterranean region. *Palaeogeography, Palaeoclimatology, Palaeoecology, 21*, 101–111.

Erba, E. (2004). Calcareous nannofossils and Mesozoic oceanic anoxic events. *Marine Micropaleontology, 52*, 85–106.

Erba, E. (2006). The first 150 million years history of calcareous nannoplankton: Biosphere–geosphere interactions. *Palaeogeography, Palaeoclimatology, Palaeoecology, 232*, 237–250.

Espitalié, J., Deroo, G., & Marquis, F. (1985a). La pyrolyse rock-eval et ses applications. *Oil & Gas Science and Technology, 40*(5), 563–579.

Espitalié, J., Deroo, G., & Marquis, F. (1985b). La pyrolyse rock-eval et ses applications. *Oil & Gas Science and Technology, 40*(6), 755–783.

Espitalié, J., Deroo, G., & Marquis, F. (1985c). La pyrolyse rock-eval et ses applications. *Oil & Gas Science and Technology, 41*(1), 73–89.

Galli, M. T., Jadoul, F., Bernasconi, S. N., & Weissert, H. (2005). Anomalies in global carbon cycling and extinction at the Triassic-Jurassic boundary: Evidence from a marine C-isotope record. *Palaeogeography, Palaeoclimatology, Palaeoecology, 216*, 203–214.

Golebiowski, R. (1990). Facial and faunistic changes from Triassic to Jurassic in the northern Calcareous Alps. *Cahiers de l'Université de Lyon, 3*, 175–184. (Série Scientifique).

Gooday, A. J. (2003). Benthic foraminifera (protista) as tools in deep-water palaeoceanography: Environmental influences on faunal characteristics. *Advances in Marine Biology, 46*, 1–90.

Gottschling, M., Renner, S. S., Meier, K. J., Willems, H., & Keupp, H. (2008). Timing deep divergence events in calcareous dinoflagellates. *Journal of Phycology, 44*, 429–438.

Götz, A. E., Ruckwied, K., Pálfy, J., & Haas, J. (2009). Palynological evidence of synchronous changes within the terrestrial and marine realm at the Triassic-Jurassic boundary (Csovár section, Hungary). *Review of Palaeobotany and Palynology, 156*(3–4), 401–409.

Gräfe, K. U. (2005). Benthic foraminifers and palaeoenvironment in the lower and middle Jurassic of the western Basque-Cantabrian basin (Nothern Spain). *Journal of Iberian Geology, 31*, 217–233.

Guex, J., Bartolini, A., Atudorei, V., & Taylor, D. (2004). High resolution ammonite and carbon-isotope stratigraphy across the Triassic-Jurassic boundary at New York Canyon (Nevada). *Earth and Planetary Science Letters, 225*, 29–41.

Hallam, A. (2002). How catastrophic was the end-Triassic mass extinction? *Lethaia, 35*, 147–157.

Hallam, A., & Wignall, P. B. (1997). *Mass extinctions and their aftermath* (p. 320). Oxford: Oxford University Press.

Hautmann, M. (2004). Effect of end-Triassic CO2 maximum on carbonate sedimentation and marine mass extinction. *Facies, 50*, 257–261.

Hautmann, M. (2008). Catastrophic ocean acidification at the Triassic-Jurassic boundary. *Neues Jahrbuch fur Geologie und Paläontologie Abhandlungen, 249*, 119–127.

Hemleben, C., Kaminski, M. A., Kuhnt, W., & Scott, D. B. (1990). *Paleoecology, biostratigraphy, paleoceanography and taxonomy of agglutinated foraminifera* (1017 pp.), vol. 327. Kluwer Academic Publishers, Dordrecht, The Netherland.

Hesselbo, S. P., Robinson, S. A., Surlyk, F., & Piasecki, S. (2002). Terrestrial and marine extinction at the Triassic–Jurassic boundary synchronized with major carbon-cycle perturbation: A link to initiation of massive volcanism? *Geology, 30*, 251–254.

Hillebrandt, A. V., & Krystyn, L. (2009). On the oldest Jurassic ammonites of Europe (Northern Calcareous Alps, Austria) and

their global significance. *Neues Jahrbuch fur Geologie und Paläontologie Abhandlungen, 253*(2–3), 163–195.

Hillebrandt, A. V., Krystyn, L., Kuerschner, W. M., et al. (2007). A candidate GSSP for the base of the Jurassic in the northern Calcareous Alps (Kuhjoch section; Karwendel Mountains, Tyrol, Austria). *ISJS Newsletter, 34*(1), 2–20.

Hillebrandt, A. V., & Urlichs, M. (2008). Foraminifera and ostracoda from the northern Calcareous Alps and the end-Triassic biotic crisis. Berichte der Geologischen Bundesanstalt, 76, Wien, pp. 30–37, 2 Abb., 2008–2009.

Hubbard, R. N., & Boulter, M. C. (2000). Phytogeography and paleoecology in western Europe and eastern Greenland near the Triassic-Jurassic boundary. *Palaios, 15*, 120–131.

Janofske, D. (1987). Kalkige Nannofossilien aus der Ober-Trias (Rhät) der Nördlichen Kalkalpen. *Berliner Geowissenschaftliche Abhandlungen, A, 86*, 45–67.

Janofske, D. (1992). Calcareous nannofossils of the Alpine upper Triassic. In: B. Hamrsmid & J. Young (Eds.), *Nannoplankton research* (pp. 87–109). Proceedings of the 4th INA conference, Prague 1991, Knihovnicka ZPN 14a, 1.

Jenkins, D. G., & Murray, J. W. (1989). *Stratigraphical atlas of fossil foraminifera* (2nd ed., p. 593). Ellis Horwood Limited: The British Micropaleontological Society.

Jones, R. W., & Charnock, M. A. (1985). 'Morphogroups' of agglutinated foraminifera: Their life positions and feeding habits and potential applicability in (palaeo) ecological studies. *Revue de Paléobiologie, 4*, 311–320.

Jorissen, F. J., De Stigter, H. C., & Widmark, J. G. (1995). A conceptual model explaining benthic foraminiferal microhabitat. *Marine Micropaleontology, 26*, 3–15.

Kaminski, M. A., Kuhnt, W., & Moullade, M. (1999). The evolution and paleobiogeography of abyssal agglutinated foraminifera since the early Cretaceous: A tale of four faunas. *Neues Jahrbuch fur Geologie und Paläontologie Abhandlungen, 212*, 401–439.

Keupp, H. (1995). Die kalkigen Dinoflagellaten—Zysten aus dem Ober-Alb der Bohrung Kirchrode 1/91 (zentrales Niedersächsisches Becken, NW-Deutschland. *Berliner Geowissenschaftliche Abhandlungen Reihe, E, 16*(1), 155–199.

Keupp, H. (2001). Palaeoenvironmental interpretation of Late Albian calcareous dinoflagellate cysts from the Kirchrode I borehole (Lower Saxony Basin, NW-Germany). *Palaeogeography, Palaeoclimatology, Palaeoecology, 174*, 251–267.

Keupp, H., & Kowalski, F.-U. (1992). Die kalkigen Dinoflagellaten-Zysten aus dem Alb von Folkestone/SE-England. *Berliner Geowissenschaftliche Abhandlungen Reihe, E, 3*, 211–251.

Keupp, H., & Mutterlose, J. (1994). Calcareous phytoplankton from the Barremian/Aptian boundary interval from NW Germany. *Cretaceous Research, 15*, 739–763.

Kohring, R., Gottschling, M., & Keupp, H. (2005). Examples for character traits and palaeoecological significance of calcareous dinoflagellates. *Paläontologische Zeitschrift, 79*(1), 79–91.

Krystyn, L., Böhm, F., Kuerschner, W. M., & Delecat, S. (2005). *The Triassic–Jurassic boundary in the northern Calcareous Alps*. In: J. Pálfy & P. Ozsvárt (Eds.), Program, abstracts and field guide. 5th field workshop of IGCP 458 project, Tata and Hallein, September 2005, pp. A1–A37.

Kuerschner, W. M., Bonis, N. R., & Krystyn, L. (2007). Carbon-isotope stratigraphy and palynostratigraphy of the Triassic-Jurassic transition in the Tiefengraben section—Nothern Calcareous Alps (Austria). *Palaeogeography, Palaeoclimatology, Palaeoecology, 244*, 257–280.

Kuhnt, W., Moullade, M., & Kaminski, M. A. (1996). Ecological structuring and evolution of deep sea agglutinated foraminifera—a review. *Revue de Micropaleontologie, 39*, 271–281.

Kuss, J. (1983). Faziesentwicklung in proximalen intraplatform-Becken: Sedimentation, Palökologie und Geochemie der Kössener Schichten. *Facies, 9*, 61–72.

Linzer, H. G., Ratschbacher, L., & Frisch, W. (1995). Tranpressional collison structures in the upper crust: The foldthrust belt of the Northern Calcareous Alps. *Tectonophysics, 242*, 41–61.

Loeblich, A. R. & Tappan, H. (1987). *Foraminiferal general and their classification* (pp. 970). Van Nostrand Reinhold compagny Inc., 1 and 2, New York.

Mailliot, S., Mattioli, E., Bartolini, A., Baudin, F., Pittet, B., & Guex, J. (2009). Late Pliensbachian—early toarcian (Early Jurassic) environmental changes in an epicontinental basin of NW Europe (Causses area, central France). A micropaleontological and geochemical approach. *Palaeogeography, Palaeoclimatology, Palaeoecology, 273*(3–4), 346–364.

Marshall, J. D. (1992). Climatic and oceanographic signals from the carbonate rock record and their preservation. *Geological Magazine, 129*, 143–160.

Martini, R., Zaninetti, L., Villeuneuve, M., Cornee, J. J., Krystyn, L., Cirilli, S., et al. (2000). Triassic pelagic deposits of Timor: Palaeogeographic and sea-level implications. *Palaeogeography, Palaeoclimatology, Palaeoecology, 160*, 123–151.

Marzoli, A., Bertrand, H., Knight, K. B., Cirilli, S., Buratti, N., Vérati, C., et al. (2004). Synchrony of the central Atlantic magmatic province and the Triassic-Jurassic boundary climatic and biotic crisis. *Geology, 32*, 973–976.

Marzoli, A., Renne, P. R., Piccirillo, E. M., Ernesto, M., Bellieni, G., & DeMin, A. (1999). Extensive 200-million-year-old continental flood basalts of the central Atlantic magmatic province. *Science, 284*, 616–618.

Mattioli, E. (1997). Nannoplankton productivity and diagenesis in the rhythmically bedded Toarcian-Aalenian Fiuminata sequence (Umbria-Marche Apennine, Central Italy). *Palaeogeography, Palaeoclimatology, Palaeoecology, 130*, 113–134.

Mattioli, E., & Pittet, B. (2004). Spatial and temporal distribution of calcareous nannofossils along proximal—distal transect in the Lower Jurassic of the Umbria–Marche Basin (central Italy). *Palaeogeography, Palaeoclimatology, Palaeoecology, 205*, 295–316.

McElwain, J. C., Beerling, D. J., & Woodward, F. I. (1999). Fossil plants and global warming at the Triassic–Jurassic boundary. *Science, 285*, 1386–1390.

McGann, M., & Sloan, D. (1999). *Benthic foraminifers in the regional monitoring program's San Francisco estuary samples: Richmond, San Francisco Estuary Institute*. San Francisco Estuary Regional Monitoring Program for trace substances, 1997, Annual Report, pp. 249–258.

McHone, J. G. (2002). Volatile emissions of central Atlantic Magmatic province basalts: Mass assumptions and environmental consequences. In: W. E. Hames & J. G. McHone, P. R. Renne, C. Ruppel (Eds.), The Central Atlantic Magmatic Province: American Geophysical Union, Geophysical Monograph *136*, 241–254.

McRoberts, C. A., Furrer, H., & Jones, D. S. (1997). Palaeoenvironmental interpretation of a Triassic–Jurassic boundary section from Western Austria based on palaeoecological and geochemical data. *Palaeogeography, Palaeoclimatology, Palaeoecology, 136*, 79–95.

Nagy, J. (1992). Environmental significance of foraminiferal morphogroups in Jurassic North Sea deltas. *Palaeogeography, Palaeoclimatology, Palaeoecology, 95*, 111–134.

Newell, N. D. (1963). Crises in the history of life. *Sciences of America, 208*, 76–92.

Noël, D., Busson, G., Cornée, A., Bodeur, Y., & Mangin, A.-M. (1994). Contribution fondamentale des coccolithophoridées à la constitution des calcaires fins pélagiques du Jurassique moyen et supérieur. *Geobios, 17*, 701–721.

Pálfy, J., Demeny, A., Haas, J., Htenyi, M., Orchard, M. J., & Veto, I. (2001). Carbon isotope anomaly at the Triassic–Jurassic boundary from a marine section in Hungary. *Geology, 29*, 1047–1050.

Raup, D. M., & Sepkoski, J. J., Jr. (1984). Periodicity of extinctions in the geological past. *Proceeding of the National Academy of Sciences of the United States of America, 81*, 801–805.

Reolid, M., Rodriguez-Tovar, F. J., Nagy, J., & Olóriz, F. (2008). Benthic foraminiferal morphogroup of mid to outer shelf environments of the Late Jurassic (Prebetic Zone, southern Spain): Characterization of biofacies and environmental significance. *Palaeogeography, Palaeoclimatology, Palaeoecology, 261*, 280–299.

Ridgwell, A. (2005). A mid Mesozoic revolution in the regulation of ocean chemistry. *Marine Geology, 217*, 339–357.

Rost, B., & Riebesell, U. (2004). Coccolithophores and the biological pump: Responses to environmental changes. In: H. R. Thierstein & J. R. Young (Eds.), *Coccolithophores: From molecular processes to global impact* (pp. 99–125). Berlin: Springer.

Ruhl, M., Kürschner, W. M., & Krystyn, L. (2009). Triassic-Jurassic organic carbon isotope stratigraphy of key sections in the western Tethys realm (Austria). *Earth and Planetary Science Letters, 281*(3–4), 169–187.

Schaltegger, U., Guex, J., Bartolini, A., Schoene, B., & Ovtcharova, M. (2008). Precise U–Pb age constraints for end-Triassic mass extinction, its correlation to volcanism and Hettangian post-extinction recovery. *Earth and Planetary Science Letters, 267*, 266–275.

Schoene, B., Guex, J., Bartolini, A., Schaltegger, U., & Blackburn, T. J. (2010). Correlating the end-Triassic mass extinction and flood basalt volcanism at the 100, 000-year level. *Geology, 38*, 387–390.

Scott, D., Gradstein, F., Schafer, C. T., Miller, A., & Williamson, M. (1983). The recent as a key to the past: Does it apply to agglutinated foraminiferal assemblages? In: J. G. Verdenius, et al. (Eds.), *Proceedings of the first workshop on arenaceous foraminifera* (pp. 147–157). 7-9 September 1981. Institute for Kontinentalsokkelundersokelser, Publ. 108.

Self, S., Thordarsen, T., Widoowson, M., & Jay, A. (2006). Volatile fluxes during flood basalt eruptions and potential effects on the global environment: A Deccan perspective. *Earth and Planetary Science Letters, 27*, 518–532.

Stanley, G. D., Jr. (2003). The evolution of modern corals and their early history. *Earth-Science Reviews, 60*, 195–225.

Stanley, G. D., Jr. (2006). Influence of seawater chemistry on biomineralization throughout phanerozoic time: Paleontological and experimental evidence. *Palaeogeography, Palaeoclimatology, Palaeoecology, 232*, 214–236.

Tanner, L. H., Hubert, J. F., Coffey, B. P., & Mcinerney, D. P. (2001). Stability of atmospheric CO_2 levels across the Triassic/Jurassic boundary. *Nature, 411*, 675–677.

Tanner, L. H., Lucas, S. G., & Chapman, M. G. (2004). Assessing the record and causes of late Triassic extinctions. *Earth-Science Reviews, 65*, 103–139.

Tanner, L. H., Smith, D. L., & Allan, A. (2007). Stomal response of swordfern to volcanogenic CO_2 and SO_2 from Kilauea volcano. *Geophysical Research Letters, 34*, L15807. doi:10.1029/2007GL030320.

Textor, C., Graf, H. F., Timmreck, C., & Robock, A. (2004). Emissions of volcanoes. In C. Granier, P. Artaxo, & C. E. Reeves (Eds.), *Emissions of atmospheric trace compounds, series: Advances in global change research, vol. 18, chapter 7* (pp. 269–304). Netherlands: Dordrecht.

Tremolada, F., Van de Schootbrugge, B., & Erba, E. (2005). Early Jurassic schizosphaerellid crisis in Cantabria, Spain: Implications for calcification rates and phytoplankton evolution across the Toarcian oceanic anoxic event, *Paleoceanography* 20. doi: 10.1029/2004PA001120.

Tyszka, J. (1994). Response of middle Jurassic benthic foraminiferal morphogroups to dysoxic/anoxic conditions in the Pieniny Klippen basin, polish carpathians. *Palaeogeography, Palaeoclimatology, Palaeoecology, 110*, 55–81.

van de Schootbrugge, B., Quan, T. M., Lindström, S., Püttmann, W., Heunisch, C., Pross, J., Fiebig, J., Petschick, R., Röhling, H. -G., Richoz, S., Rosenthal, Y., & Falkowski, P. G. (2009). Floral changes across the Triassic/Jurassic boundary linked to flood basalt volcanism. *Nature Geoscience*, ADVANCEONLINEPUBLICATION|. http://www.nature.com/naturegeoscience. doi: 10.1038/NGEO577.

van de Schootbrugge, B., Tremolada, F., Rosenthal, Y., Bailey, T. R., Feist-Burkhad, S., Brinkhuis, H., et al. (2007). End-Triassic calcification crisis and blooms of organic-walled 'disaster species'. *Palaeogeography, Palaeoclimatology, Palaeoecology, 244*, 126–141.

Villain, J. M. (1981). Les Calcisphaerulidae: Intérêt stratigraphique et paléoécologique. *Cretaceous Research, 2*, 435–438.

Wall, D., & Dale, B. (1968). Quaternary calcareous dinoflagellates (Calciodinelloideae) and their natural affinities. *Journal of Paleontology, 42*, 1395–1408.

Ward, P. D., Haggart, J. W., Carter, E. S., Wilbur, D., Tipper, H. W., & Evans, T. (2001). Sudden productivity collapse associated with the Triassic-Jurassic boundary mass extinction. *Science, 292*, 1148–1151.

Zeebe, R. E., & Westbroek, P. (2003). A simple model for the $CaCO_3$ saturation state of the ocean: The "Strangelove", the "Neritan", and the "Cretan" ocean. *Geochemistry, Geophysics, Geosystems, 4*(12), 1104. doi:10.1029/2003GC000538.

Zügel, P. (1994). Verbreitung kalkiger Dinoflagellaten-Zysten im Cenoman/Turon von Westfrankreich und Norddeutschland. *Courrier Forschungs-Institut Senckenberg,* 176, 119 pp.